Bulletin of the Seismological Society of America, Vol. 101, No. 6, pp. 2998–3019, December 2011, doi: 10.1785/0120110023

A Predictive Equation for the Vertical-to-Horizontal Ratio of Ground Motion at Rock Sites Based on Shear-Wave Velocity Profiles from Japan and Switzerland

by Benjamin Edwards, Valerio Poggi, and Donat Fäh

Abstract Ratios of vertical-to-horizontal (V/H) ground motion are important for the computation of scenario-compatible vertical design spectra. They are therefore a crucial aspect of seismic hazard analysis. We characterize the V/H ratio at rock sites in terms of the recording site's average quarter-wavelength velocity. A predictive equation is presented, which can be used for reconstructing the expected V/H ratio of the 5%-damped response and Fourier spectra for rock sites, given a known shear-wave velocity profile. The equation is based on the regression analysis of two datasets: one from Switzerland and one from Japan. The two datasets allow us to analyze well-characterized hard-rock sites in Switzerland using small earthquakes ($M_w > 2$), while the magnitude range is increased up to events of M_w 7.3 using strong-motion recordings from Japan's KiK-net seismic network. It is shown that a correlation exists between the quarter-wavelength velocity at a given frequency and the V/H ground-motion ratio. Small differences, possibly due to velocity measurement bias or topographical and basin effects, existed when analyzing the individual regional datasets. Apart from near-source distances ($R < 30$ km) for response spectra V/H, no clear magnitude- or distance-dependence of the V/H ratios is present in either of the datasets of earthquake recordings. We show that the same correlation exists for response spectra and Fourier spectra of recorded ground motion. A similar correlation was derived for ambient vibrations recorded at Swiss station sites, resulting in larger values of V/H at a given frequency and thereby indicating that V/H is sensitive to the composition of the wave field. Finally, uncertainties in the V/H models are presented. We separate the sources of uncertainty into source and site-specific components and present the single-site sigma uncertainty measure for site-specific hazard analyses.

Introduction

It is common for ground-motion prediction equations (GMPEs) to be available for predicting horizontal ground motion given a range of input parameters, such as magnitude, distance, and site class. However, in most cases the vertical component of motion is not modeled. For instance, current models based on data from Europe and the Middle East (Akkar and Bommer, 2010), the New Generation Attenuation (NGA) dataset (Abrahamson and Silva, 2008; Boore and Atkinson, 2008; Chiou and Youngs, 2008; and Chiou *et al.*, 2008), and data from Japan (Zhao *et al.*, 2006) all provide only predictions of horizontal ground motion. However, it has recently been shown that the vertical component of ground motion can have a significant effect on the seismic response of particular structures, such as bridges (e.g., Kunnath *et al.*, 2008; Gülerce and Abrahamson, 2010). A primary use of the vertical-to-horizontal ground-motion ratio (V/H) is to facilitate the prediction of response spectral ordinates (e.g., pseudospectral acceleration) for the vertical component of motion, given a GMPE derived from horizontal ground-motion data. The V/H ratio is therefore an important concept in probabilistic seismic hazard analysis (PSHA). While it may seem unusual that GMPEs are not typically available for the vertical component, it may actually be beneficial to use a GMPE for the horizontal component of motion in combination with a V/H ratio. In this case, PSHA is undertaken solely on the horizontal component of ground motion, and the resulting design spectra are later adjusted to the vertical orientation. The resulting horizontal and vertical design spectra will then both correspond to exactly the same earthquake (disaggregation) scenario (Gülerce and Abrahamson, 2011).

Newmark and Hall (1969, 1982) were among the first to propose a ratio for the scaling of vertical-to-horizontal ground motions. They proposed a V/H ratio of 2/3,

independent of period, magnitude, distance, and site condition. McGuire *et al.* (2001) proposed V/H ratios for rock sites in the United States based on existing GMPEs (western United States) and stochastic simulations (central and eastern United States). Their model was given as a function of peak ground acceleration in rock, such that increasing ground motion led to higher V/H ratios. For the western United States model they also noted a transition between around 2 and 15 Hz, where the V/H ratio increases from lower values at long periods to higher values at short periods. Since then, several studies have been undertaken with increasing model complexity, including the use of V_{S30}. See, for example, Bozorgnia and Campbell (2004), Malhotra (2006), Cauzzi and Faccioli (2008), Bommer *et al.* (2011), Gülerce and Abrahamson (2011).

V/H spectral ratios have also been studied in detail in their inverse form, the H/V ratio (e.g., Nogoshi and Igarashi, 1971). The first peak of the H/V spectral ratio is considered a reliable proxy for the estimation of the fundamental frequency of resonance (f_0) of the site S-wave transfer function (e.g., Hagshenas *et al.*, 2008, and references therein) and has been widely used in microzonation studies to characterize sediment cover, using ambient vibrations or earthquake recordings. The interpretation of the H/V spectral ratio is strongly related to the composition of the seismic wave field, which is in turn dependent both on the sources and the subsurface structure. For 1D media and ambient vibrations, H/V spectral ratios are usually interpreted as the result of surface wave propagation (Rayleigh and Love waves, fundamental or higher modes), with a significant contribution of body waves at sites exhibiting moderate to low impedance contrasts between the sediment cover and the seismic bedrock (e.g., Bonnefoy-Claudet *et al.*, 2006; Köhler *et al.*, 2007). For sites with a high impedance contrast, the typical shape of an H/V curve appears to be mainly influenced by the ellipticity function of Rayleigh waves (e.g., Yamanaka *et al.*, 1994; Fäh *et al.*, 2001). The fundamental mode, but also higher modes and Love waves, can be important. Separating the different wave contributions is not an easy task. However, special techniques (e.g., Fäh, Wathelet, *et al.*, 2009; Hobiger *et al.*, 2009; Poggi and Fäh, 2010) allow the extraction of the ellipticity of the fundamental-mode Rayleigh wave. It has also been argued that the H/V ratio is representative of the site S-wave amplification function (Nakamura, 1989), induced by resonance of shear waves trapped in the soil column. This however, has only been observed in a few cases. An identified resonance frequency in H/V ratios can also be due to 2D or 3D resonances caused by particular valley shapes (e.g., Roten *et al.*, 2006) or rock slope features (Burjánek *et al.*, 2010). In the case of 2D resonance, the resonance frequency is the same across the whole valley. As Bard and Bouchon (1985) demonstrated, the 2D fundamental frequencies of SH and SV waves are slightly above the 1D resonance frequency for shallow valleys and increase with increasing thickness to width ratio.

The influence of surface waves on the V/H ratio is significant in the frequency range above f_0. It has been shown (Scherbaum *et al.*, 2003; Albarello and Lunedei, 2009) that below this value the body wave contribution increases progressively. This is the case in soils in the frequency band below f_0 and in for rock sites in which a weathered layer is present. The S-wave resonance peak for weathered rock is generally located at rather high frequency (e.g., $f_0 > 10$ Hz for Swiss sites that were exposed to weathering after the last glaciations). At longer periods, surface waves can again contribute significantly to the wave field depending on the origin of the waves.

Recently, a novel approach to define a reference rock-velocity condition was developed by Poggi *et al.* (2011). They correlated empirical shear-wave site amplification (e.g., Edwards *et al.*, 2008; Edwards and Rietbrock, 2009; Drouet *et al.*, 2010) to the quarter-wavelength velocity profile of the site. Using the quarter-wavelength approach to compute average S-wave velocities introduced the possibility of separately analyzing amplification at different frequencies. This is not possible with classification approaches based on standard V_{S30}, National Earthquake Hazards Reduction Program (NEHRP), or Eurocode 8 (EC8). Reconstruction of the profile leading to relative-null-amplification (i.e., the reference rock) was therefore possible. In an extension of this work, we investigate the V/H ratio in terms of its relation to the average rock properties using the quarter-wavelength approximation for frequencies much lower than f_0. On the assumption that, for a rock site, the V/H ratio is controlled by characteristics of the shear-wave velocity profile, the resulting correlation between the quarter-wavelength velocity and V/H facilitates the prediction of V/H or, equally, H/V, given any specific rock-velocity profile. Our interpretation is limited to hard-rock sites, which are of principal interest in PSHA when rock ground-motions are investigated. V/H ratios due to low-velocity superficial deposits are not considered as they introduce the additional complexity of resonance within the frequency band of interest. They are also very site specific and depend on the velocity contrast between sediments and bedrock, in addition to the shape of the sediment–bedrock interface.

We investigate two regions of interest. The first is Switzerland, with its relatively dense broadband instrumentation (Deichmann *et al.*, 2010) located on hard- and very hard-rock sites (EC8 or NEHRP class A, B; Building Seismic Safety Council, 2003). In this region, 27 stations with derived shear-wave velocity profiles are available. In the case of Switzerland, mostly broadband or midperiod sensors are installed on well-studied rock sites (Fäh, Fritsche, *et al.*, 2009). However, due to the relatively low seismicity in Switzerland, the magnitude range is limited to events with $M_w < 5$. In order to both increase the robustness of the regression analysis and explore any magnitude dependence of the V/H ratio, a Japanese dataset was also analyzed. Each of the 689 sites of the dense KiK-net strong-motion network (Aoi *et al.*, 2004) includes a shear-wave velocity profile and could be used in the

analysis. While the inclusion of this data significantly increased the robustness of the results, some limitations were presented due to the simplification of some of the provided soil velocity profiles, especially at shallow depths.

V/H Ratio Data

We present the analysis of V/H ratios of ground motion in terms of both the Fourier spectra and the 5%-damped response spectra. Both Swiss and Japanese datasets are processed following the same method. The time series used are instrument corrected and include various amounts of pre-event noise. In Switzerland, the total length of recordings is limited to 100 s; generally for events recorded within 250 km, the entire wave train, including coda, is captured. In the case of Japan, the waveforms are not truncated in duration. Recorded events of any magnitude, occurring at depths of less than 25 km in Japan are included. We imposed a 25-km depth limit due to the complex tectonic environment in Japan, such that all events in our dataset can be considered shallow crustal earthquakes. In Switzerland, all earthquakes are considered shallow crustal events (with maximum depths of around 33 km). Because of the high detection threshold for the Swiss Digital Seismic Network (SDSNet), the minimum magnitude for inclusion in the analysis was set to M_L 2.0. Because of the drastically different level of seismic activity in the two regions, each dataset is covered by a different range of magnitudes. The wide overall range of recorded magnitudes (M_w 2–7.3) allows us to investigate the magnitude dependence of the V/H ratio.

Fourier spectra are computed for windows comprising of 5%–75% of the squared acceleration integral around the S wave and coda on one of the horizontal components (e.g., Raoof *et al.*, 1999, and Edwards *et al.*, 2010). Window lengths are fixed for further components of the same recording so that the frequency interval is consistent. No filtering is applied, but a mean offset removal is performed before computing the Fourier spectra. Using these Fourier spectra, along with noise estimates taken from the pre-P-wave arrival data on each recording, a signal-to-noise ratio (SNR) analysis is undertaken. This analysis assesses the bandwidth above a level equal to three times the noise. For each of the three components of a record, two values are defined: a lower and an upper frequency limit. From all components of each recording, we then selected the highest lower limit and the lowest higher limit for further processing (f_{low} and f_{high}). Between these limits, the recorded signal is considered to be dominated by the earthquake signal on all components.

For computing the response spectra, the whole time series is used. A six-pole acausal Butterworth band-pass filter is first applied (Douglas and Boore, 2010), with corner frequencies (f_{low} and f_{high}), as defined by the SNR on the three-components of motion. We define the valid frequency range of the V/H ratio based on the SNR analysis. For the Fourier spectral V/H, f_{low} is used as the lower limit. For the response spectrum f_{low} is increased by a factor of 1.2 to account for the influence of lower frequencies on a particular response spectral period (Akkar and Bommer, 2006). For the upper limit of V/H for both Fourier and response spectra, f_{high} is used. In this sense, the V/H ratios are defined purely by earthquake signals as opposed to noise.

For each record, the horizontal component used for the V/H ratio is computed from the geometrical mean of the two perpendicular horizontal Fourier or response spectra, such that

$$\frac{V}{H}(f) = \frac{V(f)}{\sqrt{H_1(f)H_2(f)}}, \tag{1}$$

where V is the vertical component and H_1 and H_2 are two perpendicular horizontal components of the Fourier or 5%-damped response spectrum. For each recording station, m, the average V/H ratio is then given by

$$\log[(\overline{V/H})_m(f)] = \frac{1}{N(f)}\sum_{n=1}^{N(f)} \log[(V/H)_n(f)], \tag{2}$$

where n denotes the n-th record of station m and $N(f)$ is the number of records available for a particular frequency at station m. Examples of V/H spectra are given in Figure 1.

Velocity Profiles and Their Quarter-Wavelength Representation

Twenty-six seismic stations of the SDSNet (Deichmann *et al.*, 2010) were used for this study. The sites were investigated as part of the PEGASOS Refinement Project (PRP; Fäh, Fritsche, *et al.*, 2009), a seismic hazard assessment project coordinated by swissnuclear (Renault *et al.*, 2010), and a microzonation project in the Basel area (Fäh and Huggenberger, 2006; Havenith *et al.*, 2007). The locations of the sites investigated during PRP were defined in order to sample the most typical rock-site conditions of seismic stations in the Swiss Alpine Foreland. Of the 27 selected station locations, 10 (all Basel stations [Havenith *et al.*, 2007], plus ZUR, SULZ, and BALST) were investigated using three-component high-resolution f-k analysis (Capon, 1969; Fäh *et al.*, 2008; Poggi and Fäh, 2010), while 17 were investigated using multichannel analysis of surface waves (Park *et al.*, 1999). Station STEIN was not used in this study, as it did not satisfy the requirement of including quarter-wavelength velocities greater than 800 m/s. For more detailed discussion and analysis of the derivation of the velocity profiles for the Swiss instrumental sites, please refer to Poggi *et al.* (2011) and references therein.

A shear-wave velocity profile of each of the 689 stations of the KiK-net strong-motion network was provided by the Japanese National Research Institute for Earth Science and Disaster Prevention (NIED, see Data and Resources section). These profiles have been obtained from downhole logging on boreholes set up for buried sensor installation (Fujiwara *et al.*, 2004). The maximum depth reached is highly variable, depending on the particular station and spans from a few tens

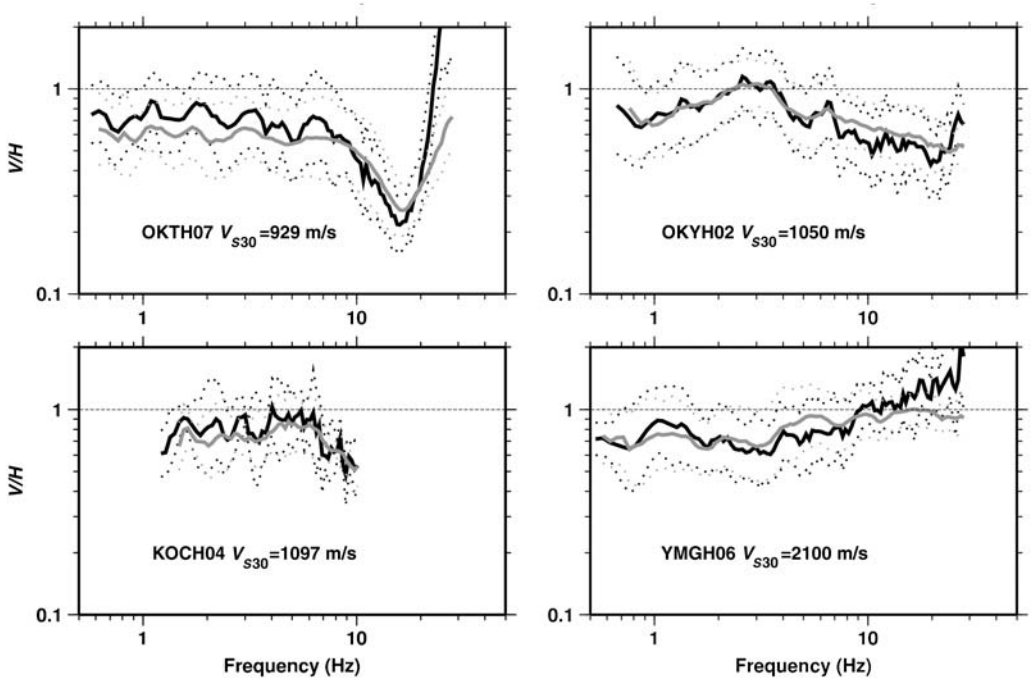

Figure 1. V/H spectral ratios for four Japanese stations used in the study. Black, Fourier spectra; gray, 5%-damped response spectra; solid line, mean; dotted lines, ±1 standard deviation. The minimum and maximum frequencies were limited by the SNR of the earthquake recordings.

of meters to about 200 m. Each profile consists of a limited number of discrete layers (generally from 4 to 7), for which an estimate of the S and P velocities is provided. There is a wide range of surface velocity types, from soil to very hard rock. Of these sites, 498 were used in this study, with selection based on quarter-wavelength velocities greater than 800 m/s. Unfortunately, an estimation of uncertainties was not provided for the Japanese profiles.

The quarter-wavelength velocity profiles for the Swiss and Japanese sites are computed following Joyner *et al.* (1981) and Boore (2003). The reader is referred to Poggi *et al.* (2011) for a complete description of the method; however, the following briefly outlines the procedure. The quarter-wavelength method assumes that any vertically heterogeneous soil profile can be characterized, at a given frequency, by an equivalent two-layer model in which the interface is located at a depth corresponding to one-quarter of the wavelength of interest:

$$z(f) = \frac{V_s^{\text{average}}(z)}{4f} = \frac{V_s^{\text{QWL}}(f)}{4f}. \tag{3}$$

The equivalent layer has a travel-time average velocity ($V_s^{\text{QWL}}(f)$) computed over the input profile, down to that specific depth $z(f)$. The computation of the average quarter-wavelength velocity, $V_s^{\text{QWL}}(f)$, at a specific frequency can then be obtained through the minimization of

$$\arg\min_{z(f)} \left\| z(f) - \frac{V_s^{\text{QWL}}(f)}{4f} \right\|, \tag{4}$$

given that

$$V_s^{\text{QWL}}(f) = z(f)\left[\int_0^{z(f)} \frac{1}{V_s(z)}\,dz\right]^{-1}. \tag{5}$$

This is achieved through a direct search approach over z in order to recursively converge to the solution of the minimization problem. For the Swiss locations, we used the same profiles as used in Poggi *et al.* (2011). For the Japanese stations, quarter-wavelength velocity profiles were calculated based on the profiles provided by NIED.

The investigation of increasingly long-period (and thus long-wavelength) V/H ratio values requires the knowledge of increasingly deep velocity profiles. However, each site is characterized only to a limited depth, depending on the investigation technique employed. It is therefore necessary to extrapolate the required information from the available data below this limit. Adding new layers to the existing velocity models (e.g., using some gradient or power-law function) would involve numerous assumptions. To produce a justifiable estimation, we therefore proceed as follows. The quarter-wavelength velocity functions are computed down to a frequency (f^{Max}) corresponding to a maximum available profile depth. The thickness of the last layer is usually undefined in the model, so we generally impose a lower depth bound, corresponding to a percentage of the second-to-last-layer depth (here 50%). The derived quarter-wavelength profile is then extended to lower frequencies through cubic interpolation of the existing points (Fig. 2). A clear advantage of this procedure is that such an extrapolation produces a smooth average velocity profile, which is constrained by the velocity variation of the uppermost layers. Clearly, the lower the extrapolated frequency range is, the higher the

level of uncertainty on the results. Therefore, we define an empirical frequency range (f^{Ext}) for the extended quarter-wavelength profile, such that

$$f^{\mathrm{Max}} > f^{\mathrm{Ext}} \geq 0.5 f^{\mathrm{Max}}. \quad (6)$$

An overview of all quarter-wavelength velocity profiles, normalized by the frequency corresponding to a threshold velocity of 800 m/s, is presented in Figure 3 for both the Swiss and Japanese data.

Correlation of V/H with Quarter-Wavelength Velocity

V/H ratios of both Fourier spectral amplitudes and 5%-damped response spectra (pseudospectral acceleration) were compared with the corresponding quarter-wavelength velocity over frequencies from 0.5 to 20 Hz. For inclusion in the regression of V/H ratio versus quarter-wavelength velocity, the V/H measure needed to be based on at least five records, whilst the quarter-wavelength velocity had to be

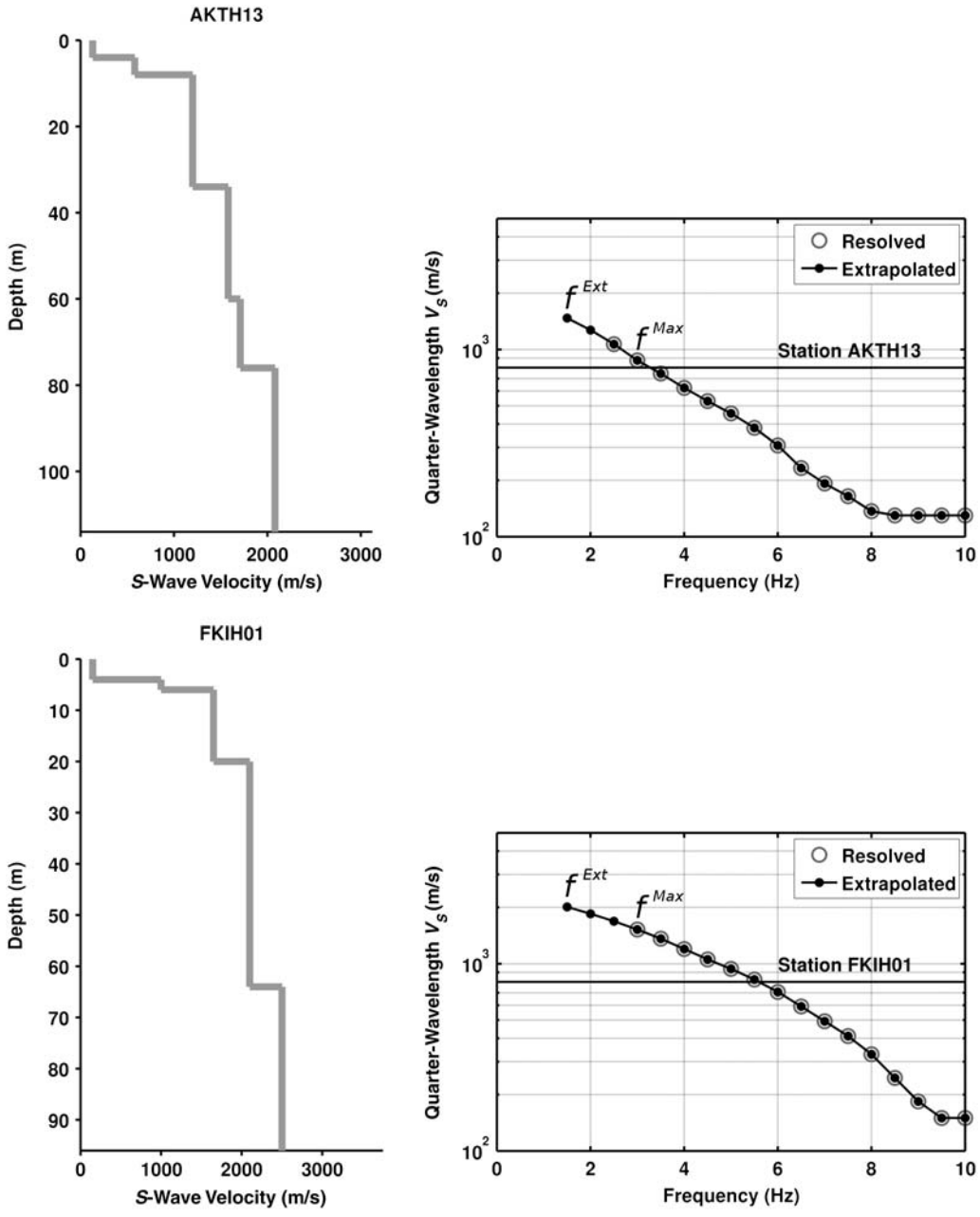

Figure 2. (Right) Example of quarter-wavelength velocity versus frequency for two profiles of the Japanese KiK-net network, along with (left) the corresponding shear-wave velocity profiles. It is possible to notice the effect of extrapolating the quarter-wavelength velocity profile beyond the resolved depth, as indicated by f^{Ext} and f^{Max}. The 800 m/s velocity threshold for inclusion in the regressions is indicated as a horizontal black line.

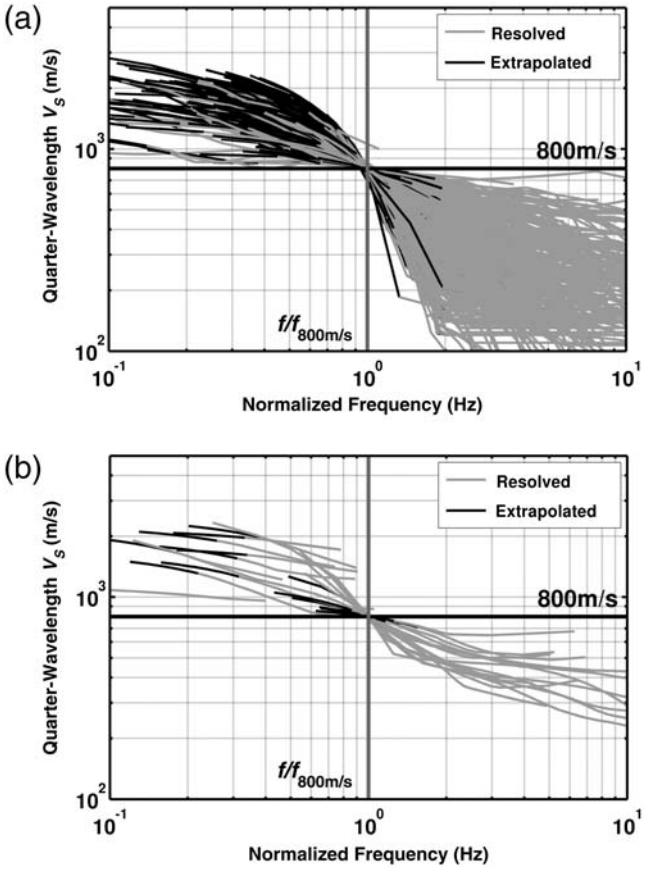

Figure 3. Ensemble of all processed quarter-wavelength velocity versus normalized frequency for (a) Japanese profiles and (b) Swiss profiles. Normalized frequency refers to that corresponding to the threshold quarter-wavelength velocity of 800 m/s (as indicated by the horizontal black line).

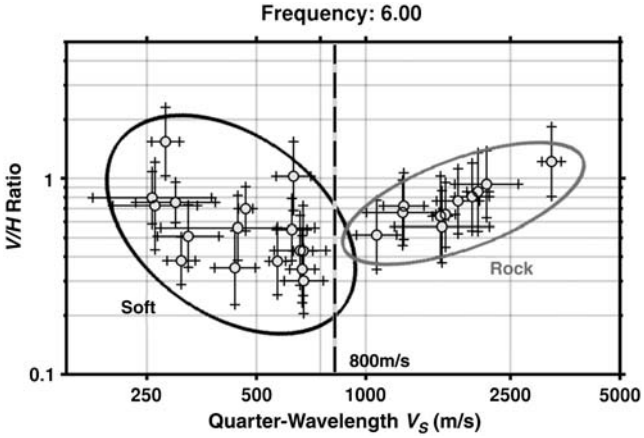

Figure 4. Example correlation of V/H ratio with the quarter-wavelength velocity at 6 Hz for Swiss sites. A quarter-wavelength velocity threshold of 800 m/s is defined in order to separate the different contributions of soft sediments and rock sites in the correlation. For lower velocities, resonance effects might be dominant and lead to unwanted effects in the regression.

greater than or equal to 800 m/s. This lower limit of quarter-wavelength velocity is defined in order to separate the different contributions of soft sediments and rock sites in the correlation. For lower velocities, resonance effects might be dominant and lead to unwanted effects in the regression (Fig. 4). At the lowest frequencies, a limiting factor for data availability is the maximum depth of the velocity profile, while for the highest frequencies it is the resolution of the upper layers' velocities. A regression for the best fitting linear relation between the logarithms of quarter-wavelength velocity and V/H ratio was performed using a least-squares minimization. The form of the equations was

$$\ln\left[\frac{V}{H}(f)\right] = a(f)\ln\left[V_s^{\mathrm{QWL}}(f)\right] + b(f). \qquad (7)$$

Switzerland

We used 5384 records to define the V/H ratios of the 26 Swiss sites used in the regression. Minimum available frequencies ranged from 0.1 to around 10 Hz, while maximum frequencies ranged from 5 to 50 Hz, depending on the noise present in the recording (Fig. 5a). The recordings sampled a wide range of hypocentral distances, spanning 5–300 km (Fig. 5b). Earthquakes with magnitudes between 2 and 5.5 and depths between 0 and 33 km were used (Fig. 5c).

An example of the correlation between quarter-wavelength velocity and V/H ratio of Fourier spectral amplitude for the Swiss sites is plotted in Figure 6 for frequencies 1, 2.5, 5, and 10 Hz. Figure 7 shows the same correlations for 5%-damped response spectra. The regression results are detailed in Table 1. Frequencies between 4 and 8 Hz tended to lead to the smallest standard deviations relative to the regression. It is possible that this is due to the resolution of the *S*-wave velocity profiles from multichannel analysis of surface waves (MASW) used in this study. For instance, an average velocity of 800 m/s down to 50 m corresponds to the lower 4 Hz frequency in the quarter-wavelength representation. Greater depths, with velocities becoming less well resolved by the MASW, correspond to lower frequencies. For frequencies above 8 Hz, we increasingly enter the limited resolution of the uppermost layers of the velocity profile. Figure 8 shows the regression results for frequencies between 1 and 10 Hz. Frequencies outside this range were considered unreliable. The unreliable velocity profile at depth leads to uncertainty at low frequencies, whereas the limited number of data points with velocity higher than 800 m/s in the upper layers, in addition to the limited resolution of the velocity profiles in the uppermost layer, leads to uncertainty at high frequencies.

With the exception of the 1-Hz fit, the regression results of all frequencies up to 10 Hz converge at quarter-wavelength velocities around 2000 m/s (Fig. 8). All fits have a positive gradient, with the V/H ratio changing from around 0.5 at 800 m/s to 0.9 at 2500 m/s. Some frequency dependence can be observed, with higher gradients at lower frequencies. For the 5%-damped response spectra, a similar

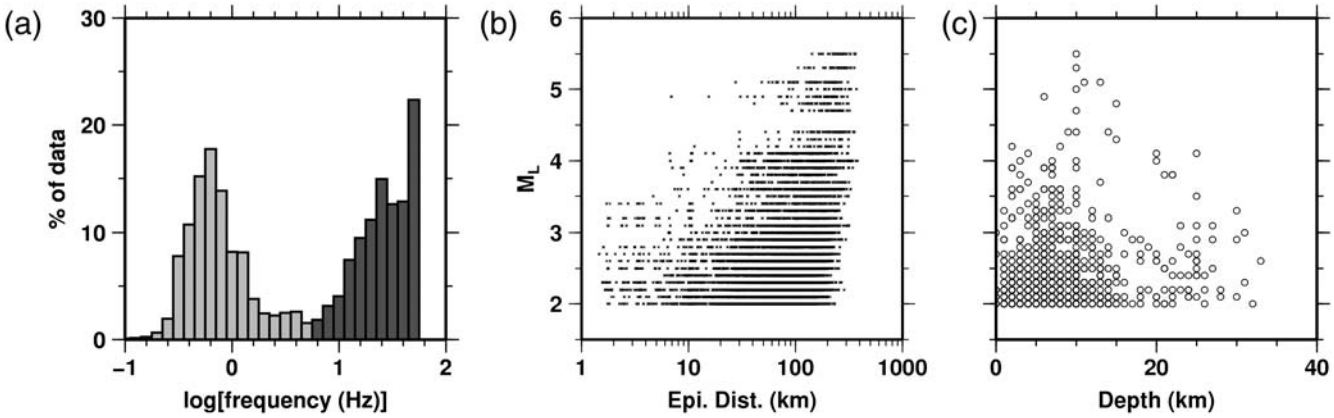

Figure 5. Data coverage in terms of (a) frequency (light gray, minimum; dark gray, maximum), (b) epicentral distance, and (c) earthquake depth for the recordings used to define the V/H ratio of the 26 Swiss sites.

observation can be made (Fig. 7, Table 1). Again, the best fits are obtained for frequencies between 4 and 8 Hz, although frequencies of 2–10 Hz all produce robust results. The regression results and misfits of both the V/H from Fourier spectral amplitude and response spectra are very similar (Fig. 8).

Japan

The Japanese dataset includes significantly more data than the Swiss: 78,419 records were used to compute the V/H ratios of 498 sites, which included quarter-wavelength velocities of greater than 800 m/s. The maximum frequency was limited to 30 Hz, due to the low-pass filter applied at the recording site (Aoi *et al.*, 2004). The resulting range of frequencies available in the data, after checking the SNR, was between 0.1 and 30 Hz (Fig. 9a). The lower bound ranged from 0.1 to around 5 Hz, whereas the upper bound ranged from 5 to 30 Hz; 3379 events with M_{JMA} (Japanese Meteorological Agency magnitude) between 1.9 and 7.3 were used (Fig. 9b), with hypocentral depths ranging from 0 to 25 km (Fig. 9c). A trend of increasing minimum epicentral distance with magnitude is present (Fig. 9b), as often seen due to triggering, occurrence rates, and SNR constraints (e.g., Zhao *et al.*, 2006).

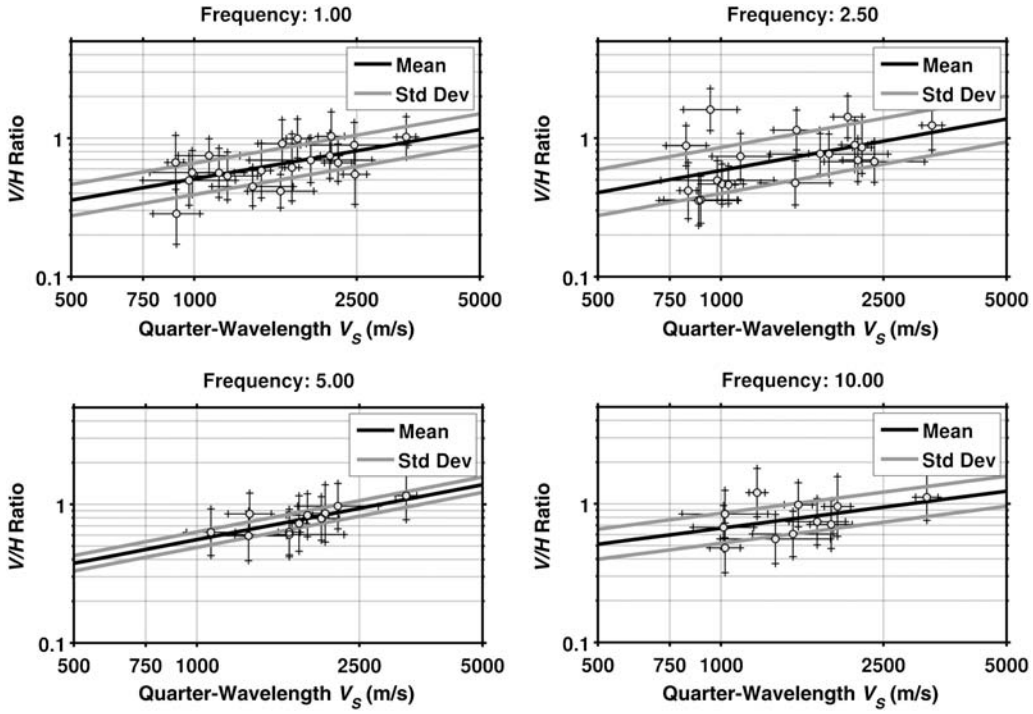

Figure 6. Correlation of V/H ratio of Fourier spectral amplitudes and quarter-wavelength velocities at selected frequencies for the Swiss dataset.

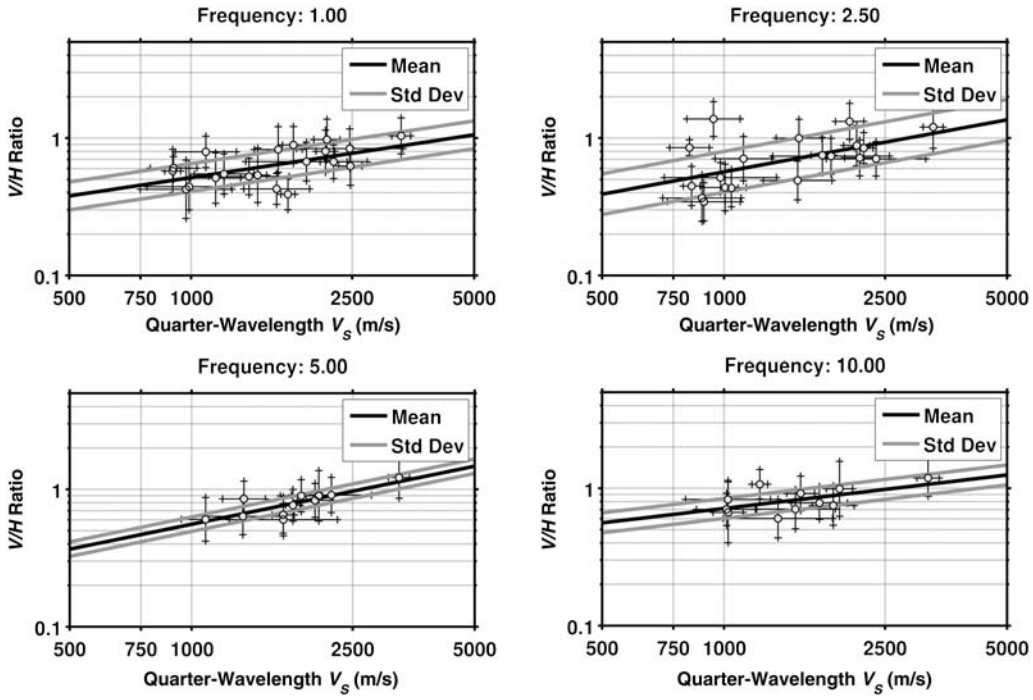

Figure 7. Correlation of V/H ratio of 5%-damped response spectra and quarter-wavelength velocity for the Swiss dataset for selected frequencies.

An example of the correlation between V/H ratio of Fourier spectra and quarter-wavelength velocity is shown in Figure 10. The regression results are detailed in Table 2. It is evident that most points are available to the regression for frequencies between approximately 1 and 5 Hz. Below and above these frequencies, the number of data points decreases. Additionally, for lower frequencies, more points are deemed to have unresolved quarter-wavelength velocity,

Table 1
Regression Results for the Swiss Data

Frequency (Hz)	Fourier Spectra					5%-Damped Response Spectra				
	a	b	σ(ln)	Number of Stations	Nonextrapolated	a	b	σ(ln)	Number of Stations	Nonextrapolated
0.75	0.4471	−3.7068	0.2674	21	4	0.5441	−4.4422	0.2327	21	4
1	0.4884	−4.0452	0.2668	20	3	0.4329	−3.6503	0.2364	20	3
1.5	0.5828	−4.7051	0.2429	20	3	0.5616	−4.5542	0.2506	20	3
2	0.5755	−4.5929	0.3050	20	3	0.6002	−4.7814	0.2950	20	3
2.5	0.5275	−4.1802	0.3832	19	2	0.5384	−4.2844	0.3427	19	2
3	0.5333	−4.2555	0.3531	18	3	0.5704	−4.5263	0.3434	18	3
3.5	0.6385	−5.0267	0.3212	16	3	0.6198	−4.8909	0.3297	16	3
4	0.6140	−4.8680	0.1438	13	3	0.6669	−5.2509	0.1342	13	3
4.5	0.6505	−5.1469	0.1505	12	3	0.6186	−4.8785	0.1315	12	3
5	0.5675	−4.5070	0.1286	11	2	0.6043	−4.7589	0.1214	11	2
5.5	0.6876	−5.4161	0.1061	11	3	0.6369	−4.9977	0.1056	11	3
6	0.7001	−5.5146	0.1078	11	4	0.6303	−4.9431	0.1013	11	4
6.5	0.5875	−4.6324	0.1055	11	4	0.5878	−4.6093	0.1011	11	4
7	0.5050	−3.9822	0.1066	11	6	0.5284	−4.1461	0.0992	11	6
7.5	0.4693	−3.7218	0.1242	11	7	0.4723	−3.7153	0.1014	11	7
8	0.4332	−3.4621	0.1594	11	8	0.4212	−3.3278	0.1137	11	8
8.5	0.4051	−3.2537	0.1935	11	9	0.3804	−3.0171	0.1311	11	9
9	0.4044	−3.2440	0.2160	11	10	0.3590	−2.8485	0.1461	11	10
9.5	0.4104	−3.2792	0.2333	11	10	0.3534	−2.7951	0.1577	11	10
10	0.3827	−3.0490	0.2498	11	10	0.3486	−2.7458	0.1669	11	10

Parameters a and b refer to Equation 7. σ(ln), the natural log standard deviation of the regression; Number of Stations, the total number of stations used in the regression; Nonextrapolated, the number of stations used that did not have their quarter-wavelength velocity extrapolated at that given frequency.

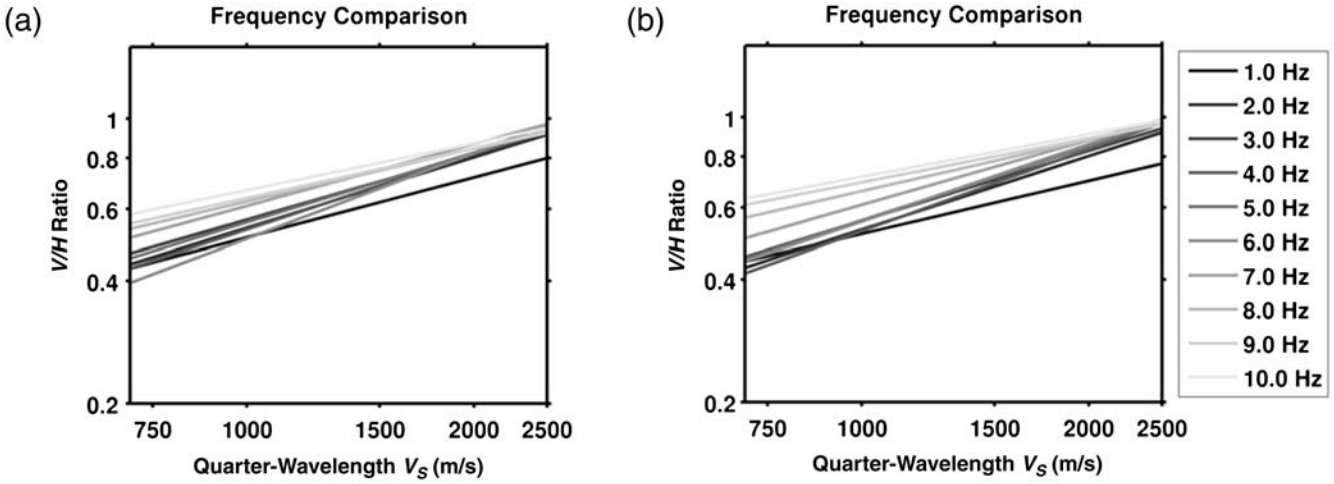

Figure 8. Regression results of the quarter-wavelength velocity versus V/H for (a) Fourier spectral amplitude and (b) 5%-damped response spectra at Swiss sites for frequencies between 1 and 10 Hz.

where the value was computed based on extrapolation from higher frequencies, as described in the section Velocity Profiles and Their Quarter-Wavelength Representation.

The fit of V/H from response spectra (Fig. 11, Table 2) is similar to that of the Fourier spectra, as observed for the Swiss data. However, on comparing the regression results, there are slight differences (Fig. 12). The general trend, as found with the Swiss data, is for increasing quarter-wavelength velocity to lead to higher V/H ratio over all frequencies. As with the regression of Swiss data, a systematic variation in the results with frequency can be observed. However, in this case the trend is in the opposite sense, with higher frequencies leading to lower V/H ratios. For the response spectra V/H, all frequencies approach a common ratio of around 0.7 for quarter-wavelength velocities of 2000 m/s. This is lower than the value of 0.9 at the same quarter-wavelength velocity seen for the Swiss sites. For the Fourier spectra V/H, the convergence of the different frequency regressions is not as clear. For lower quarter-wavelength velocities, the V/H ratio of both Fourier and response spectra decreases, down to around 0.4 for 800 m/s.

Regional Variability

Ideally, a unique relation for the V/H ratio would be available. However, the results of independent regressions of Swiss and Japanese sites suggest small differences between the regions (Fig. 13). Clearly the results using the Japanese data can be considered more robust, simply due to the volume of data available. However, the quality of the Japanese velocity profiles was unknown because only one profile is provided for each site, without any uncertainty on the velocity estimation. Conversely, the Swiss data were limited in quantity, but the velocity profile data included the estimation of uncertainty. As an initial test, a subjective selection of the Japanese sites was undertaken, in order to include only those considered to be of higher quality. The selection was based on the comparison of the theoretical SH- and quarter-wavelength amplification functions, with the shape of the H/V function at each site. The idea was to identify those profiles with a clear mismatch between the measured and the modeled fundamental frequency of resonance. Around 18% of sites were removed where the peak in the theoretical SH-amplification

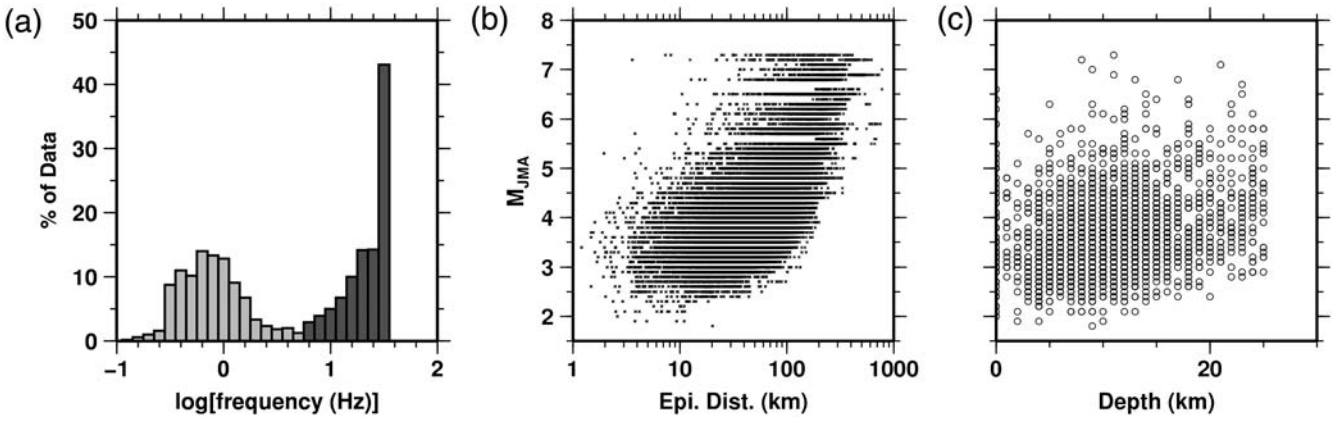

Figure 9. Data coverage in terms of (a) frequency (light gray, minimum; dark gray, maximum), (b) epicentral distance, and (c) earthquake depth for the recordings used to define the V/H ratio of the 498 Japanese sites.

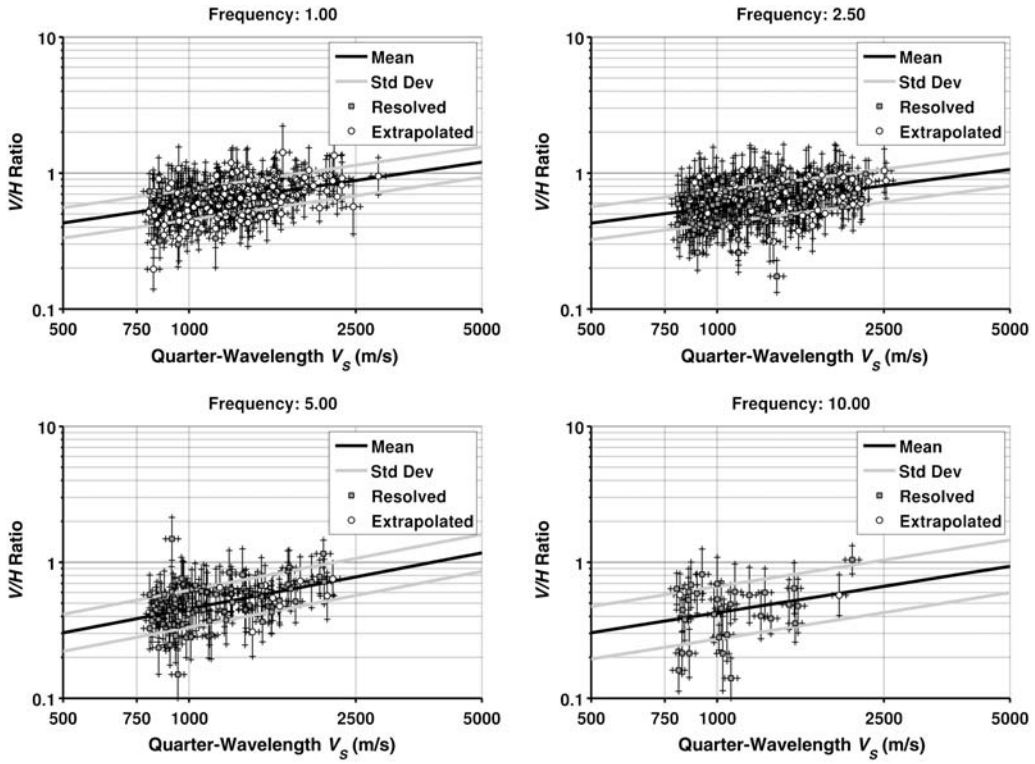

Figure 10. Correlation of V/H ratio of Fourier spectral amplitude and quarter-wavelength velocity for the Japanese dataset at selected frequencies. "Resolved" points are those for which the quarter-wavelength depth is within the velocity profile. "Extrapolated" points are based on extrapolated quarter-wavelength velocity.

Table 2
Regression Results for the Japanese Data

Frequency (Hz)	Fourier Spectra					5%-damped Response Spectra				
	a	b	σ(ln)	Number of Stations	Nonextrapolated	a	b	σ(ln)	Number of Stations	Nonextrapolated
0.5	0.2481	−2.3008	0.3049	32	6	0.0143	−0.6765	0.3007	30	5
0.75	0.3292	−2.8012	0.2724	104	10	0.2285	−2.1305	0.2510	81	10
1	0.4467	−3.6204	0.2575	184	27	0.4013	−3.3999	0.2441	176	26
1.5	0.4203	−3.4552	0.2223	250	59	0.4090	−3.5038	0.2444	243	59
2	0.4232	−3.4757	0.2454	249	92	0.4406	−3.7297	0.2577	249	92
2.5	0.3948	−3.3011	0.2789	219	107	0.4307	−3.6717	0.2770	218	107
3	0.4200	−3.5288	0.2978	182	111	0.4984	−4.1854	0.2980	182	111
3.5	0.4450	−3.7496	0.3109	154	105	0.5248	−4.3822	0.3100	154	105
4	0.4387	−3.7430	0.3148	125	102	0.4814	−4.0677	0.3178	125	102
4.5	0.5222	−4.3715	0.3213	114	101	0.5249	−4.3909	0.3261	111	98
5	0.5874	−4.8439	0.3142	93	84	0.5914	−4.8681	0.3038	92	83
5.5	0.6228	−5.0910	0.3298	83	75	0.5723	−4.7120	0.3113	83	75
6	0.5641	−4.6862	0.3303	68	63	0.4925	−4.1412	0.3182	66	61
6.5	0.6156	−5.0796	0.3392	60	56	0.5380	−4.4796	0.3311	60	56
7	0.6248	−5.1610	0.3575	56	52	0.5639	−4.6802	0.3429	56	52
7.5	0.4625	−3.9983	0.3669	48	44	0.4398	−3.7893	0.3566	48	44
8	0.5533	−4.6736	0.3791	44	41	0.5312	−4.4572	0.3695	44	41
8.5	0.4097	−3.6716	0.4082	41	38	0.4185	−3.6615	0.3836	41	38
9	0.4708	−4.1206	0.4670	37	35	0.4609	−3.9679	0.4157	37	35
9.5	0.5835	−4.9319	0.4908	35	33	0.5433	−4.5599	0.4305	35	33
10	0.4886	−4.2292	0.4450	32	30	0.4579	−3.9418	0.4067	32	30

Parameters a and b refer to Equation 7. σ(ln), the natural log standard deviation of the regression; Number of Stations, the total number of stations used in the regression; Nonextrapolated, the number of stations used that did not have their quarter-wavelength velocity extrapolated at that given frequency.

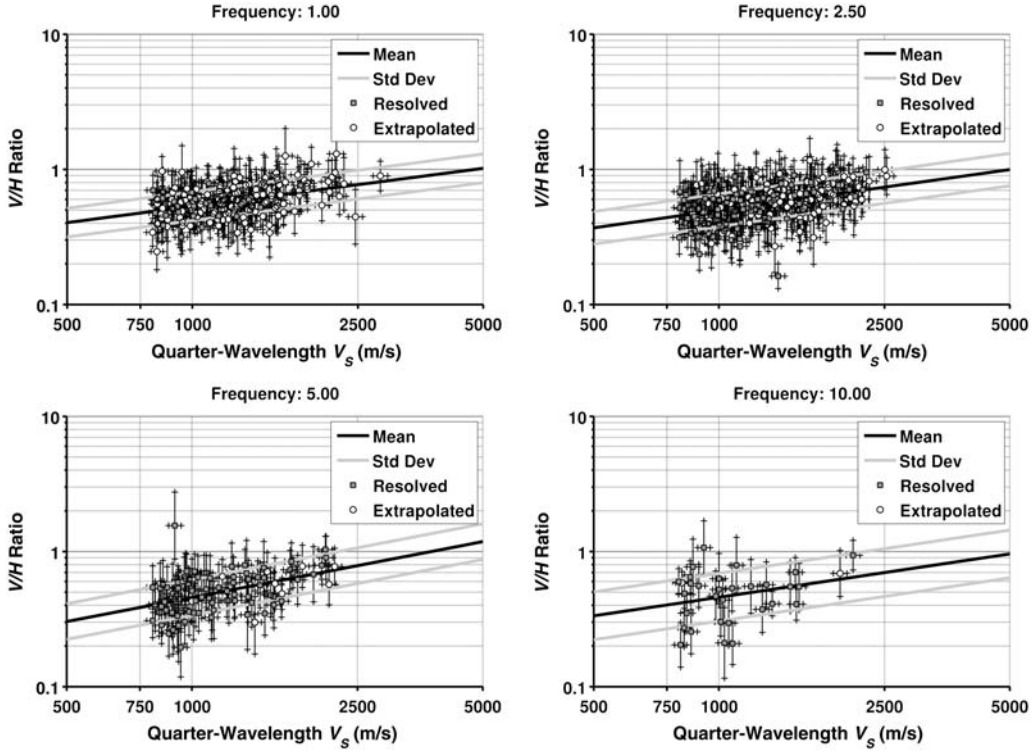

Figure 11. Correlation of V/H ratio of 5%-damped response spectra and quarter-wavelength velocity for the Japanese dataset at selected frequencies. "Resolved" points are those for which the quarter-wavelength depth is within the velocity profile. "Extrapolated" points are based on extrapolated quarter-wavelength velocity.

function was very different from the measured H/V peak. This resulted in small changes in the frequency band up to 7 Hz, but larger deviations above 7 Hz (Fig. 13).

In order to test the statistical significance of the different regression results, we established a hypothesis test. The null hypothesis was a single quarter-wavelength–V/H model, with data from both Swiss and Japanese regions sampling a unique model. In this case the differences observed in the regression results would be simply due to insufficient sampling of the model space. The alternative hypothesis is that two unique models exist, with each region sampling a different quarter-wavelength–V/H model. Student's t-test was employed to evaluate the null hypothesis. For this test it was postulated that the more substantial Japanese dataset leads to a model closer to the true single model. The test was employed for the Fourier spectra quarter-wavelength–V/H model: as the response spectrum is simply a multiplication of the Fourier spectrum with the response of a simple harmonic oscillator, we expect that, given a unique model for the Fourier domain, a unique model will also exist in the response spectral domain. For each site of both the Swiss and Japanese regions, the V/H ratio was reconstructed from the

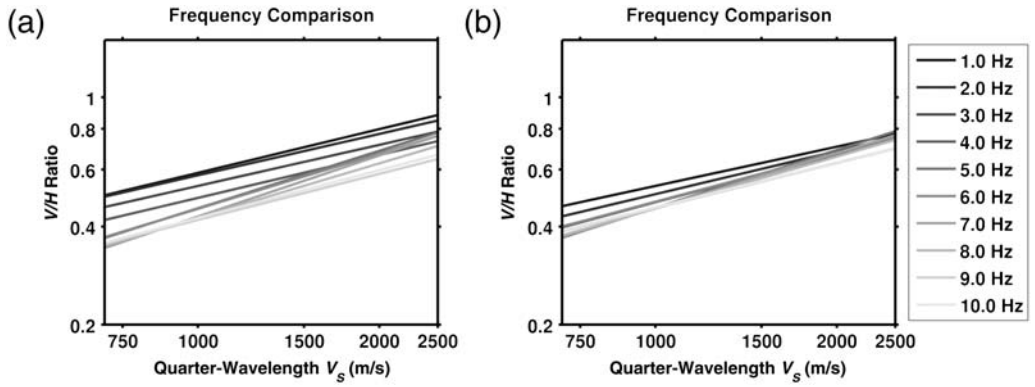

Figure 12. Regression results of the quarter-wavelength velocity versus V/H for (a) Fourier spectral amplitude and (b) 5%-damped response spectra at Japanese sites for frequencies between 1 and 10 Hz.

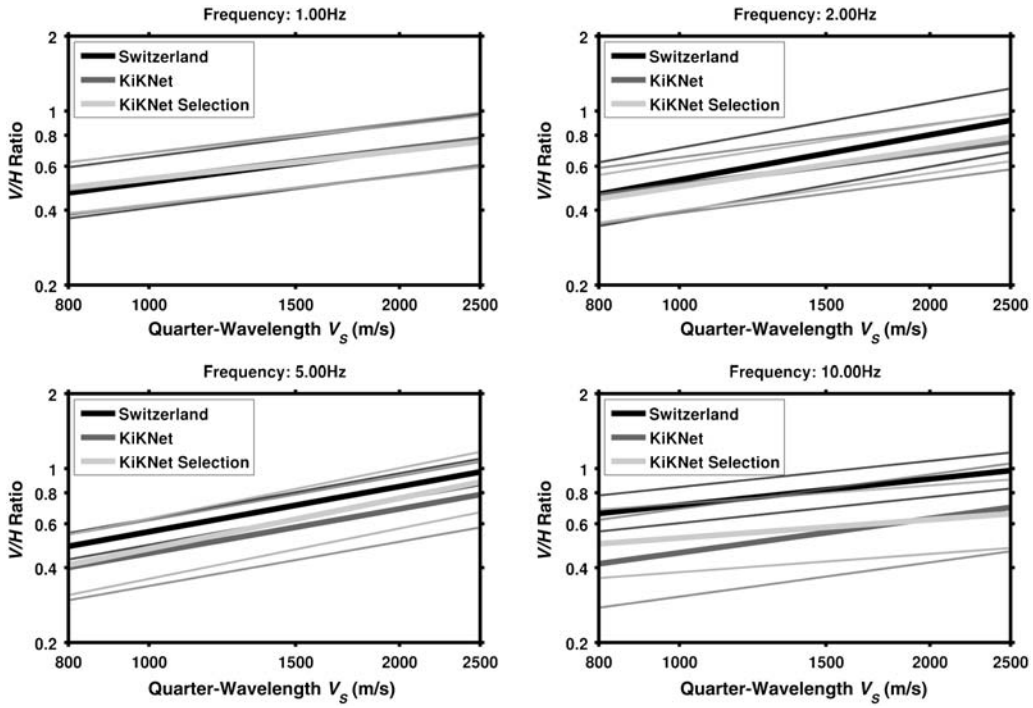

Figure 13. Comparison of regression results between V/H ratios of response spectra and quarter-wavelength velocity for Switzerland, Japan, and a subset of the Japanese data. The thick lines indicate the mean, while the dotted lines show the standard deviation of data relative to the mean.

site's quarter-wavelength velocity profile using the Japanese regression results (Fig. 14).

In order to group all sites into a single analysis, the residual misfit between the real and computed V/H ratio was analyzed rather than the actual V/H values for a range of frequencies between 1 and 10 Hz. Student's t-test was performed individually at 25 log-spaced frequencies, with

$$t(f) = \frac{\mu_J - \mu_S}{\sqrt{\frac{1}{n_J} + \frac{1}{n_S}}\sqrt{\frac{(n_J-1)\sigma_J^2 + (n_S-1)\sigma_S^2}{n_J+n_S-2}}}. \quad (8)$$

μ_J and μ_S are the mean of the residual misfit between the real and back-computed V/H functions for Japan and Switzerland, respectively. n_J and n_S are the number of stations available at each respective frequency, while σ_J^2 and σ_S^2 are the variance of the residual misfit for the Japanese and Swiss sites, respectively.

By definition, $\mu_J \approx 0$ (as the Japanese model was derived using the Japanese data), thus the mean residual misfit is negligible. Essentially, the test describes how close the Swiss V/H data are to fitting the Japanese model, considering the data quantity and standard deviations. In order to obtain a measure of confidence, the resulting values, $t(f)$, can be compared with values computed for a particular combination of degree of freedom and probability (Fig. 15). Depending on the degree of confidence required to reject the null hypothesis, different frequencies can be considered to be consistent with a single quarter-wavelength–V/H model. If requiring a 95% confidence, we cannot reject the single model hypothesis between frequencies of around 1.2 and 6.5 Hz.

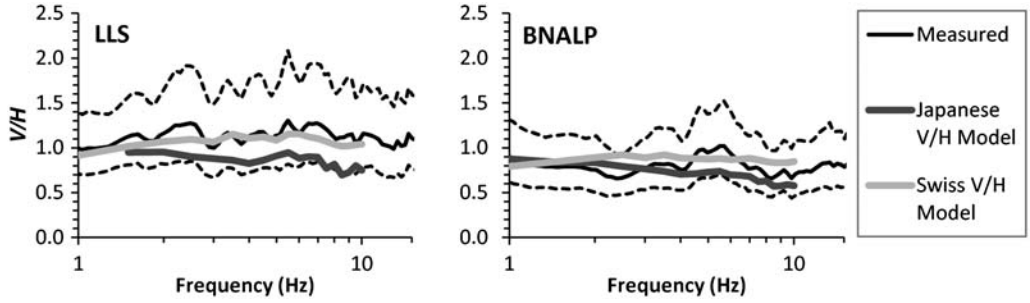

Figure 14. Comparison of measured Fourier spectra V/H ratios versus the Swiss and Japanese models for two Swiss sites, BNALP and LLS. The mean (solid) and ±sigma (dashed) curves are given for the measured V/H.

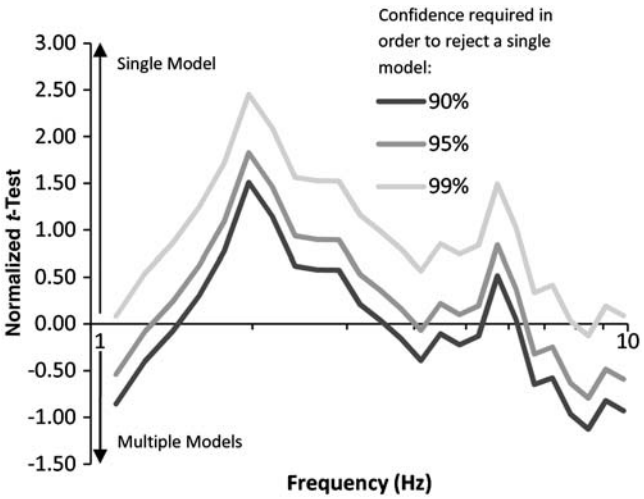

Figure 15. Normalized *t*-test values versus frequency for different confidence limits. Positive normalized *t*-test values indicate that the null hypothesis (a single V/H model) cannot be rejected at the relevant confidence level.

The statistical tests showed that, in the lower frequency range (1 to 7 Hz), a single model can be used for the prediction of V/H based on the quarter-wavelength velocity representation at a site. Given the differences in the trend of V/H with frequency in the two models (Figs. 8 and 12), it can therefore also be considered that a frequency-independent relation is appropriate in this range. It could be that the differences at higher frequencies arise due to the peculiarities of a region. For example, in Switzerland, many sites are located in regions with strongly varying topography, such as on mountains. On the other hand, in Japan many sites are located directly on thin soil layers, even if the underlying rock is very hard. Other reasons for the differences are discussed later.

V/H Dependence on Magnitude and Distance

Among others, Bozorgnia and Campbell (2004), Bommer *et al.* (2011) and Gülerce and Abrahamson (2011) presented models for the V/H ratio based on a range of parameters such as earthquake magnitude, slip type, rupture distance, and site characterization in terms of V_{S30}. Gülerce and Abrahamson found that, in addition to V_{S30}, the V/H ratio was dependent on the recording distance and weakly dependent on magnitude. In order to assess if this dependence was present in our data, we performed residual analysis on the back-computed V/H functions (Fig. 14) for all sites with points having a quarter-wavelength velocity greater than 800 m/s (Fig. 4). The regressions of quarter-wavelength velocity versus V/H of response and Fourier spectra were used to reconstruct the expected V/H ratio at each of our sites. Using these predicted V/H ratios, we could compare a range of recorded V/H ratios, at different magnitudes and distances, to the expectation. Any dependence should then be evident in residual plots. Plots of residual versus magnitude, distance, and frequency are shown in Figure 16.

For the Fourier spectra V/H, we found no evidence for magnitude or distance dependence of the V/H ratio. It should be noted that, due to the different magnitude scales employed by the Swiss and Japanese agencies, there may be systematic differences in M between the two datasets. However, the only consequence of this to the residual plot in Figure 16 is that densities could be shifted horizontally (M changes). As there is already no trend present with magnitude, this could not affect our interpretation. Below 15 km, there is a slight departure from a nonzero residual (e.g., approximately 4% at 10 km), but, considering the limited data coverage in this range, it is difficult to conclude its significance. On the other hand, the response spectra V/H show a slight trend with distance. At 30 km the V/H ratios are about 5% lower, whereas at 190 km, the V/H ratios are, on average, about 5% higher than the model predicts. This trend, however, is only present in the Japanese data. Because of the distance–magnitude distribution in the Japanese data, this trend is also reflected in the magnitude residual plot. Further analysis confirmed that the trend was only with distance and not magnitude. In order to rule out interplay between residuals (e.g., opposing residual trends with different parameters), we looked at the data in small bins of different frequency, magnitude, and distance in order to assess if any systematic variation or trends were apparent. This was not the case, and the trends always appeared (as presented) for all the data combined. Nevertheless, considering the standard deviation, the variation is so small that it should not be overinterpreted. At near-source hypocentral distances ($R_{\text{hyp}} < 30$ km), the variation of V/H with distance is more pronounced for response spectra (Fig. 17), with V/H around 18% lower than the model at 10 km. A correction for this near-field effect (δ_r) was computed by producing a linear fit to the mean V/H residual versus distance within 30 km. This led to

$$V/H_{R_{\text{Corr}}} = \delta_r \frac{V}{H} = 10^{(4.13.10^{-3} R_{\text{hyp}} - 0.127)} \frac{V}{H}, \quad R_{\text{hyp}} \leq 30 \text{ km}. \tag{9}$$

The correction is only applicable to the response spectra V/H model. Further analysis of individual frequency ranges indicated that this near-field correction was specifically applicable to lower frequencies (i.e., up to 5 Hz). For higher frequencies, the mean residual became more scattered and showed less systematic deviation. Beyond 10 Hz, no near-field systematic trend was observed in the residual misfit. The decrease in V/H in the near-field response spectra, and not in the Fourier spectra, may be due to an increase in strong horizontally orientated pulses, such as *S*-wave phases.

Frequency-Independent Correlation of Quarter-Wavelength and V/H Ratio

Statistical tests suggest that, between ~1 and 7 Hz, a unique model exists that can explain the relation between

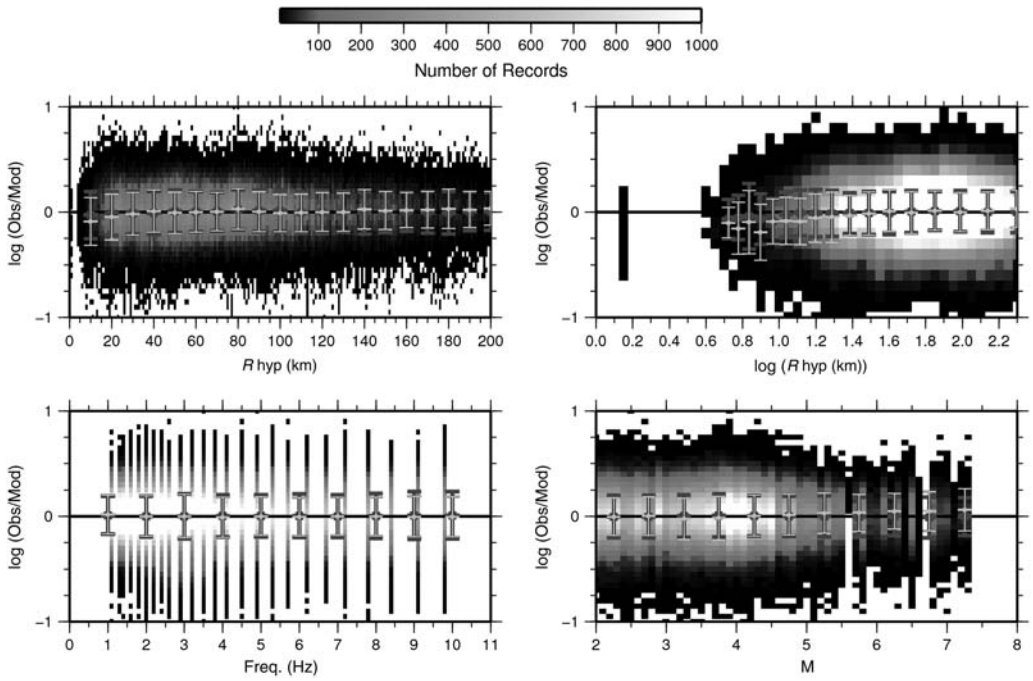

Figure 16. Residual analysis of recorded V/H (labeled Obs) versus V/H reconstructed using the quarter-wavelength velocity model (labeled "Mod") for the V/H data. The individual regional models are used. Plots of residual misfit (log(Obs/Mod)) are shown for R_{hyp} (hypocentral distance), $\log(R_{\text{hyp}})$, frequency, and M (M_{JMA} for Japanese data; M_{L} for Swiss data). The error bars (dark gray, Fourier spectra; light gray, response spectra) indicate the mean and standard deviation of the residuals at various intervals of each parameter.

V/H and the quarter-wavelength velocity in both the Swiss and Japanese datasets. As the frequency dependence of the V/H relation was in the opposite sense for the two regions, it can also be inferred that a frequency-independent relation should fit the combined data equally well in this frequency range. Such a model has the advantage that it is also easy to implement. The form is given by

$$\ln\left[\frac{V}{H}(f)\right] = a\ln[V_s^{\text{QWL}}(f)] + b. \qquad (10)$$

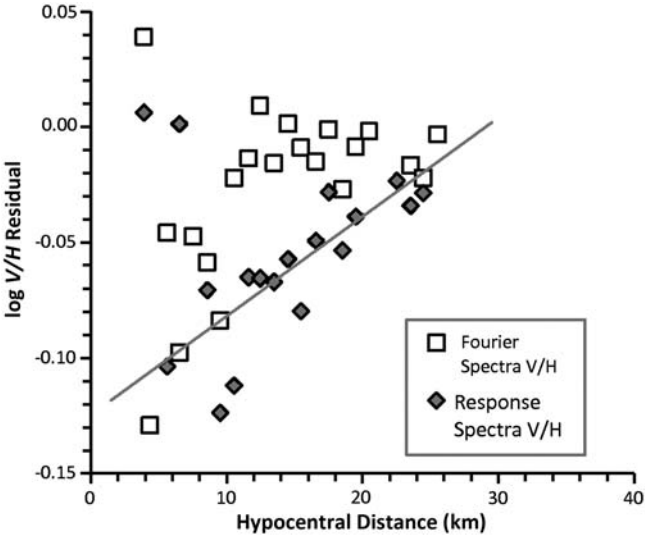

Figure 17. Mean near-source V/H ratio residuals (over the range 1–10 Hz) for Fourier and response spectra. The linear fit is to the response spectra data (equation 9).

In the following, we produce a frequency-independent V/H–quarter-wavelength velocity relation for the individual regions, in addition to a combined average model. To reduce bias in the results, which may occur due to the reduced data coverage of both low and high frequencies, a synthetic dataset was produced, based on the individual frequency regressions (Tables 1 and 2). For the average model, based on data from both Japan and Switzerland, the resampled dataset also reduces the bias due to the significantly larger size of the Japanese dataset.

Resampling of the datasets was made at 10 quarter-wavelength velocities between 800 and 2500 m/s. One-thousand predictions were made at each quarter-wavelength velocity for frequencies 1–7 Hz, in steps of 0.5 Hz. A random component was introduced in order to account for the standard deviation of the original regression (Tables 1 and 2). The resulting data were then inverted for a frequency-independent relation between quarter-wavelength velocity and the V/H ratio. The regression results are given in Tables 3 and 4. The models are compared in Figure 18. The difference between the Fourier and response spectra V/H models is very small. The variation between the Swiss and Japanese results mimics the differences discussed for the frequency-dependent regressions, while the combined model provides an intermediate model. Figure 18 also shows a comparison of the combined model with the model of Gülerce

and Abrahamson (2011) for M_w 6.5 at 30, 50, and 100 km. The comparison of the model of Gülerce and Abrahamson (2011) with quarter-wavelength velocity is possible through the use of corresponding V_{S30} and frequency pairs, where the quarter-wavelength frequency is given by

$$f = \frac{V_S^{\mathrm{QWL}}(z(f))}{4z(f)} = \frac{V_{S30}}{120}. \tag{11}$$

The match in some cases is reasonable, with increasing V/H with quarter-wavelength velocity. However, for increasing magnitude or decreasing distance, the V/H values given by Gülerce and Abrahamson (2011) increase and vice versa. The majority of their values do, however, consistently fall within the standard deviation of our model.

The residual misfit of the data to the V/H model is shown in Figure 19. The correction for the response spectra in the near field (equation 9) is applied. Note that, as we now use the frequency-independent regression model, the residuals are not forced to have zero mean at all frequencies (as was the case for Fig. 16). Nevertheless, even well beyond the frequencies used in the combined frequency regression (1–7 Hz), and up to 25 Hz (limited by the data bandwidth), the residual misfit is still reasonable. In order to improve the high-frequency fit of this model further, we propose a simple adjustment (δ_f) based on the residual analysis, such that

$$V/H_{hf\mathrm{Corr}} = \delta_f \frac{V}{H} = \frac{(V/H)}{0.722 + 0.9672\exp(-0.176f)}, \quad f > 7 \text{ Hz}. \tag{12}$$

This correction is valid for the Fourier spectra and response spectra V/H models. It is consistent with the results of others, such as McGuire *et al.* (2001), Bommer *et al.* (2011), and Gülerce and Abrahamson (2011), who also found higher V/H at frequencies greater than approximately 10 Hz.

Modelling the Uncertainty of V/H

The contribution of uncertainty is important in PSHA. So far the V/H–quarter-wavelength velocity regressions were presented with uncertainty based on average V/H ratios at a particular site. This uncertainty, therefore, does not represent the true variability of V/H ratios on a record-to-record basis. Furthermore, it is useful to present uncertainty of ground-motion parameters in terms of their interevent, intraevent, and site variability for PSHA studies (Alatik *et al.*, 2010). Assuming normal statistics, the total uncertainty of the V/H model is given by

$$\sigma^2 = \frac{1}{N}\sum_{n=1}^{N}\{Y_n - \ln[f_n(\mathbf{X_{es}}, \mathbf{\Theta})]\}^2, \tag{13}$$

where Y_n is the natural log of the V/H ratio and $f_n(\mathbf{X_{es}}, \mathbf{\Theta})$ is that predicted by the model at a given frequency for observation n. $\mathbf{X_{es}}$ is the vector of independent parameters (in this case the frequency and corresponding quarter-wavelength velocity) and $\mathbf{\Theta}$ is the vector of model parameters (the coefficients of the regression; e.g., from Tables 3 or 4, together with the corrections in equations 9 and 12). This can be split into inter- (between) and intra- (within) event terms, τ and ϕ, respectively:

$$\sigma = \sqrt{\tau^2 + \phi^2}. \tag{14}$$

The intraevent term ϕ is then split into intersite and intrasite terms, ϕ_{S2S} and ϕ_{SS}, respectively:

$$\phi = \sqrt{\phi_{SS}^2 + \phi_{S2S}^2}. \tag{15}$$

This formulation is very useful for site-specific hazard analyses, where the so-called single-site sigma is more representative of variability at the site because it removes the contribution to uncertainty by using numerous sites in the derivation of models:

Table 3
Regression Results for the Frequency-Independent Fourier Spectra V/H Model (Equation 10)

Switzerland			Japan			Combined		
a	b	σ(ln)	a	b	σ(ln)	a	b	σ(ln)
0.589	−4.677	0.247	0.502	−4.155	0.327	0.546	−4.416	0.296

σ(ln) is the natural log standard deviation of the regression.

Table 4
Regression Results for the Frequency-Independent Response Spectra V/H Model (Equation 10)

Switzerland			Japan			Combined		
a	b	σ(ln)	a	b	σ(ln)	a	b	σ(ln)
0.584	−4.631	0.238	0.498	−4.163	0.314	0.541	−4.397	0.291

σ(ln) is the natural log standard deviation of the regression.

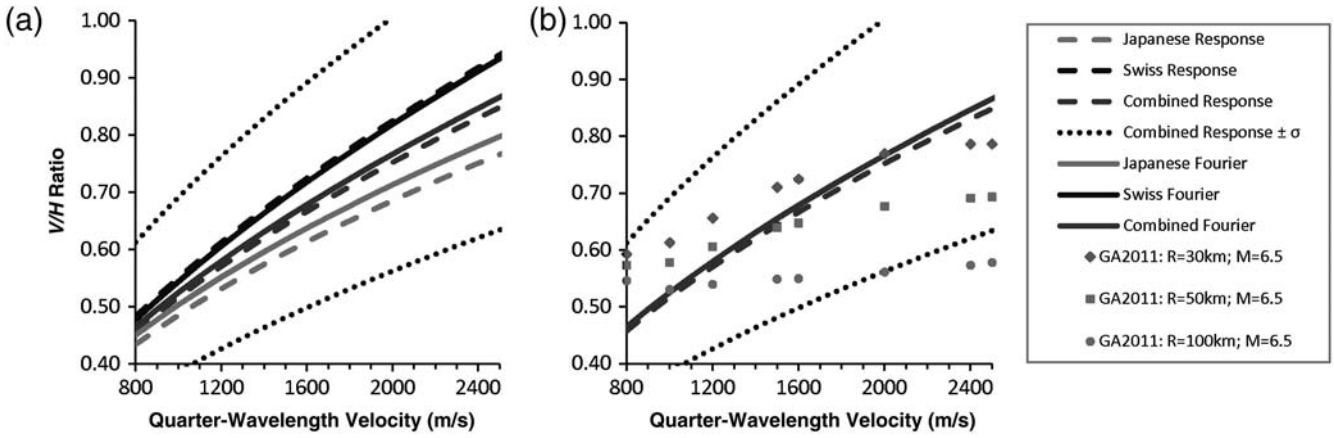

Figure 18. (a) Comparison between the Swiss, Japanese, and combined frequency-independent V/H–quarter-wavelength velocity relation models for the Fourier and response spectra. The standard deviation (±sigma) is indicated for the combined response spectra V/H model. (b) The combined frequency-independent V/H–quarter-wavelength velocity model is compared to the model of Gülerce and Abrahamson (2011 (GA2011) for M_w 6.5, with $R_{rup} = 30$, 50, and 100 km, using V_{S30} and frequency corresponding to the given quarter-wavelength velocity.

$$\sigma_{SS} = \sqrt{\phi_{SS}^2 + \tau^2}. \quad (16)$$

For the V/H model, we chose to use the frequency-independent V/H–quarter-wavelength correlation of the individual regions instead of the combined region model so as not to add any uncertainty that may be related to systematic bias in velocity measurement techniques or regional differences. It should be noted that we also applied the high-frequency and close distance corrections (equations 9 and 12) to the model, where applicable. The models are compared to the respective data between 1 and 7 Hz (both Fourier and 5%-damped response spectra), as this is the target range of the combined frequency V/H–quarter-wavelength model. The resulting uncertainty values are presented in Table 5 for the Fourier spectra model and Table 6 for the response spectra V/H model. All measures of uncertainty tended to

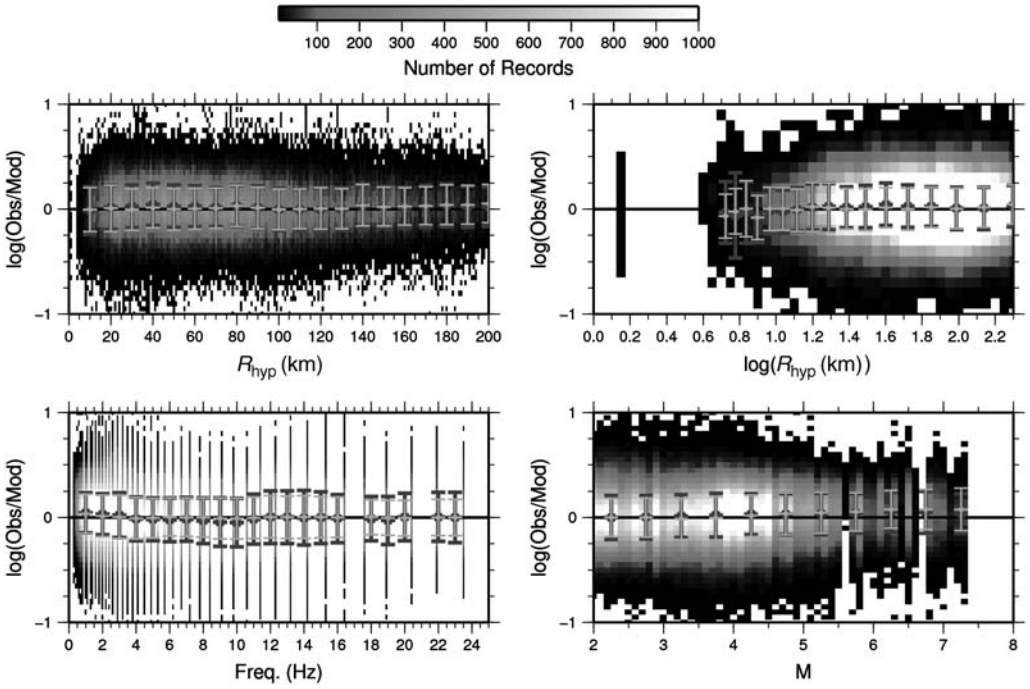

Figure 19. Residual analysis of recorded V/H (labeled "Obs") versus V/H, reconstructed using the frequency-independent V/H–quarter-wavelength velocity relation (labeled "Mod") for the V/H data. The corrections for near-field response spectra V/H (equation 9) and high-frequency V/H (equation 12) are applied. Plots of residual misfit (log(Obs/Mod)) are shown for R_{hyp} (hypocentral distance), log(R_{hyp}), frequency, and M (M_{JMA} for Japanese data; M_L for Swiss data). Frequencies from 1–7 Hz are included in all plots. In the frequency plot, frequencies up to 25 Hz are also included. The error bars (dark gray, Fourier spectra; light gray, response spectra) indicate the mean and standard deviation of the residuals at various intervals of each parameter.

Table 5
Uncertainty for the Combined Frequency Response Spectra V/H Model

	Hypocentral Distance (km)																			
	0–200 km					0–30 km					30–100 km					100–200 km				
M	σ	τ	ϕ_{S2S}	ϕ_{SS}	σ_{SS}	σ	τ	ϕ_{S2S}	ϕ_{SS}	σ_{SS}	σ	τ	ϕ_{S2S}	ϕ_{SS}	σ_{SS}	σ	τ	ϕ_{S2S}	ϕ_{SS}	σ_{SS}
2.0–7.3	0.510	0.259	0.240	0.368	0.450	0.540	0.375	0.232	0.311	0.487	0.494	0.246	0.244	0.352	0.430	0.457	0.231	0.221	0.327	0.400
2.0–4.5	0.518	0.263	0.257	0.365	0.450	0.536	0.374	0.227	0.310	0.485	0.496	0.254	0.256	0.341	0.425	0.447	0.233	0.232	0.303	0.382
4.5–7.3	0.457	0.167	0.244	0.348	0.386	0.581	0.392	0.304	0.303	0.495	0.448	0.158	0.259	0.330	0.366	0.443	0.199	0.226	0.324	0.380

Uncertainties are given in natural log units. Values are given for different magnitude and distance ranges, as indicated.

Table 6
Uncertainty for the Combined-Frequency Fourier Spectra V/H Model

	Hypocentral Distance (km)																			
	0–200 km					0–30 km					30–100 km					100–200 km				
M	σ	τ	ϕ_{S2S}	ϕ_{SS}	σ_{SS}	σ	τ	ϕ_{S2S}	ϕ_{SS}	σ_{SS}	σ	τ	ϕ_{S2S}	ϕ_{SS}	σ_{SS}	σ	τ	ϕ_{S2S}	ϕ_{SS}	σ_{SS}
2.0–7.3	0.479	0.183	0.215	0.387	0.428	0.514	0.285	0.195	0.380	0.475	0.468	0.181	0.216	0.374	0.416	0.473	0.206	0.209	0.371	0.424
2.0–4.5	0.484	0.187	0.219	0.389	0.431	0.511	0.284	0.190	0.380	0.474	0.471	0.186	0.217	0.375	0.418	0.485	0.212	0.223	0.375	0.430
4.5–7.3	0.457	0.137	0.226	0.373	0.397	0.539	0.301	0.250	0.371	0.477	0.452	0.132	0.236	0.363	0.386	0.457	0.175	0.209	0.367	0.407

Uncertainties are given in natural log units. Values are given for different magnitude and distance ranges, as indicated.

be lower for the subset of data using only magnitudes greater than 4.5. The interevent variability was higher in the range 0–30 km, which is consistent with the complexity and variation of near-source wave propagation. Intrasite variability was the least variable measure, when varying the magnitude and distance selection. This suggests that the deconvolution of uncertainty is robust, as this measure should indeed be independent of magnitude and distance because it is a purely site-related parameter. It should be noted that the uncertainty measure of the Fourier spectra V/H may be influenced by processing steps such as smoothing or, as in this case, the use of multitaper fast-Fourier-transform algorithms. Table 7 shows the variation in uncertainty (in terms of the factorial difference) with varying frequency, even beyond the frequencies used in the derivation of the model. Even at frequencies controlled only by the empirical aspect of the model (i.e., above 7 Hz), the uncertainties remain low and even generally decrease. This may be due to the stochastic nature of the high-frequency wave field.

Noise

The use of ambient noise is a common means of obtaining the H/V ratio at a site. So far, we have compared only the V/H ratios obtained from earthquake recordings. We now explore the possibility of the equivalence, or indeed difference, between V/H ratios of earthquake recordings and ambient noise. For the 26 Swiss sites used in the analysis, noise measurements were compiled. For the broadband installations, around 10 hours of noise were taken from the continuous datastream, comprised of 5 minutes each day between January and April at 02:00. For the strong-motion installations, noise recordings of around one hour duration were made using 5-s velocimeters. The data were carefully checked for spikes, outages, earthquakes, and any other issues. The data were then processed in the same way as the earthquake recordings. V/H was then correlated with the quarter-wavelength velocity, as before. The resulting regressions are plotted in Figure 20b. A comparison with the results from the Fourier V/H from earthquakes (Fig. 20a) shows a constant shift in the amplitude of the V/H ratio obtained from the different sources. Noise measurements lead to V/H ratios that are higher (by a factor of around 1.5 at 800 m/s) than that seen in earthquake recordings. For the higher quarter-wavelength velocities, this difference becomes less apparent.

The differences between V/H ratios observed for earthquake recordings and noise recordings may be caused by the different compositions of the wave fields. In earthquake recordings, the incident wave field arrives from a restricted range of azimuths, whereas for ambient vibrations and high frequencies, waves arrive at the same time from different directions. For the low-frequency range of ambient vibrations (below 1 Hz), the range of azimuths of the incident waves is also limited due to the ocean sources. Such effects of the azimuth might be tested by comparing different processing of V/H spectral ratios (e.g., Fäh *et al.*, 2010).

For a given frequency, high quarter-wavelength velocities relate to longer wavelengths, and we might therefore expect a higher surface-wave contribution to the wave field. Indeed, more comparable V/H ratios for earthquake recordings and ambient vibrations are observed at low frequency. Further experimentation would be required to test whether body waves contribute more at low quarter-wavelength velocities for ambient vibrations than for earthquakes at a particular site.

The difference in the composition of the wave field might be a reason for the difference in V/H ratios obtained for the Swiss and the Japanese datasets at frequencies above 1 Hz (Fig. 13). For instance, the difference could be caused by systematic differences in the average site condition in the two datasets. Swiss sites have a tendency to be close to a theoretical rock site where body waves, in particular *P* waves, might contribute more to the wave field at high frequency. On the other hand, Japanese sites include a number of locations in or close to deep basins for which surface-wave excitation might significantly contribute to the wave field.

Table 8 shows the results of a regression for equally sampled distributions from each of the individual frequency regressions between 1 and 7 Hz for the noise data, as was done for the earthquake data. This relation could be used for the reconstruction of quarter-wavelength velocity profiles based on ambient noise measurements.

Table 7
Correction Factors for Obtaining Frequency-Specific Uncertainties

	M = 2–7.3, R = 0–200 km				
f (Hz)	$\nu(\sigma)$	$\nu(\tau)$	$\nu(\phi_{S2S})$	$\nu(\phi_{SS})$	$\nu(\sigma_{SS})$
0.5–3.5	0.968	0.924	0.988	0.981	0.962
3.5–6.5	0.990	0.894	1.136	0.968	0.944
6.5–9.5	0.940	0.899	1.117	0.875	0.883
9.5–12.5	0.859	0.776	0.961	0.852	0.828
12.5–15.5	0.782	0.682	0.913	0.767	0.740
15.5–25.5	0.799	0.670	0.895	0.814	0.769

These values should be multiplied with the values in Tables 5 or 6 to obtain frequency-specific uncertainty.

Discussion and Conclusions

We showed that, in the log-space, the V/H ratio at a given frequency was linearly related to the corresponding site's quarter-wavelength velocity over a suite of over 450 Japanese and 26 Swiss sites. A frequency-independent parameterization of the relation was presented. In addition, a correction for V/H of near-field response spectra and V/H at high frequencies was included, purely based on observational misfit to the initial quarter-wavelength model. The model is completely independent of earthquake magnitude. The final V/H model, including single-site uncertainty (σ_{SS}), is

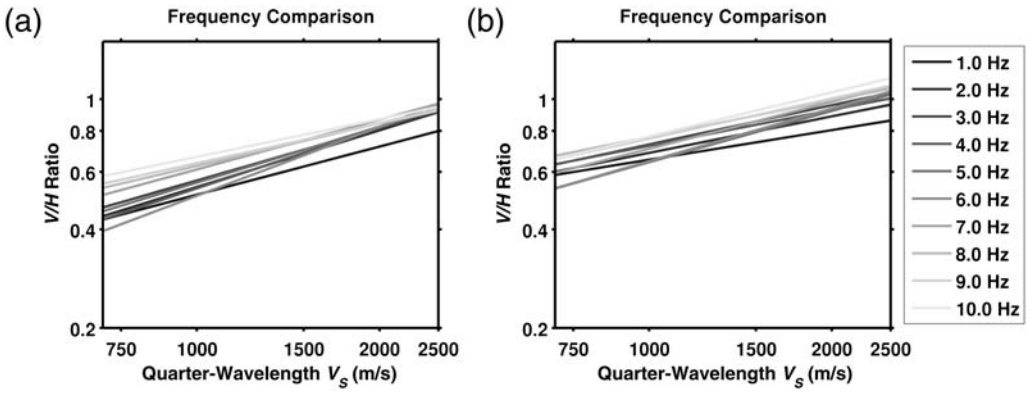

Figure 20. Regression results of the quarter-wavelength velocity (in m/s) versus V/H for (a) Fourier spectral amplitude from earthquake recordings and (b) Fourier spectral amplitude from ambient noise recordings at Swiss sites for frequencies between 1 and 10 Hz.

$$\ln\left(\frac{V}{H}\right) = \ln(\delta_r \delta_f) + [a \ln(V_s^{\mathrm{QWL}}) + b] \pm \sigma_{\mathrm{SS}}, \tag{17}$$

with

$$\begin{aligned}
&\delta_r = 10^{(4.13.10^{-3} R_{\mathrm{hyp}} - 0.127)} && \text{for response spectra with } R_{\mathrm{hyp}} \leq 30 \text{ km},\\
&\delta_r = 1 && \text{for response spectra with } R_{\mathrm{hyp}} > 30 \text{ km or Fourier spectra},\\
&\delta_f = 1 && \text{for } f \leq 7 \text{ Hz},\\
&\delta_f = \frac{1}{0.722 + 0.9672 \exp(-0.176 f)} && \text{for } f > 7 \text{ Hz},
\end{aligned}$$

and a and b given by the combined model in Table 3 for Fourier spectra and Table 4 for response spectra. σ_{SS} can be taken from Tables 5 or 6, depending on the spectrum type, while the correction factors in Table 7 can be used to adjust the uncertainty for selected frequency ranges.

Frequency-dependant models were initially established for the Swiss and the Japanese regions separately. Both models displayed similar features, principally that the general trend was for V/H values around 0.5 at 800 m/s increasing to values between 0.8 and 1.0 at 2500 m/s. The frequency dependence of the models displayed trends in the opposite sense, with increasing V/H with frequency for Switzerland and decreasing V/H with frequency for Japan (relative to a given quarter-wavelength velocity). It was noted, however, that limitations in both datasets may lead to a degree of uncertainty in the regressions at individual frequencies. The magnitude- and distance-dependence of the V/H ratio was also explored. Moment magnitudes between 2 and 7.3, and distances up to 200 km were tested. We compared the measured V/H ratio with the model and found that, contrary to other models, there was no systematic dependence on either magnitude or distance. However, for near-source distances ($R < 30$ km), the response spectra V/H were generally lower than the initial model. This was not observed for the Fourier spectra V/H. This may be due to strong horizontally oriented pulses; for example, S-wave phases being present in the near field. An adjustment to the response spectra V/H model was presented to account for this.

Statistical tests showed that the regressions for individual frequencies were robust for the frequency range of 2–7 Hz but were more unstable for the highest frequencies (i.e., greater than around 10 Hz). However, such high frequencies are often associated with the uppermost layers of the velocity profile in the quarter-wavelength representation. These upper layers may not always be properly resolved. We showed that at 95% confidence we could not discard a null hypothesis of a single V/H model for both regions between 1 and 7 Hz. We computed a synthetic dataset that sampled the two regional frequency-dependent models equally. Three frequency-independent relations between V/H and quarter-wavelength velocity were then produced: a Swiss, a Japanese, and a combined model for both Fourier and 5%-damped response spectra. These frequency-independent relations leave all variation of the V/H ratio with frequency to the quarter-wavelength velocity profile. The three models lead to similar relations. These frequency-independent relations can be used for the prediction of the V/H ratio at given rock sites with

Table 8
Regression Results for the Frequency-Independent Fourier Spectra V/H Model of Ambient Noise (Equation 10)

a	b	σ(ln)
0.430	−3.344	0.223

σ(ln) is the natural log standard deviation of the regression.

known velocity profile. The prediction can be extended to purely theoretical profiles, which may be defined as a reference condition for hazard analysis. When using the frequency-independent V/H–quarter-wavelength relations at high frequencies (e.g., $f > 10$ Hz, which were not included in our original analysis due to their association with very shallow surface layers), it was seen that the V/H ratio was underpredicted. A correction for this was produced that is consistent with the observations of others, such as McGuire *et al.* (2001).

A similar correlation between V/H and the quarter-wavelength velocity was derived for ambient vibrations recorded at Swiss station sites. These resulted in larger values of V/H at a given frequency. This may indicate that V/H depends on the composition of the wave field in terms of a ratio between surface waves and body waves (P and S waves), the distribution of azimuths of incidence, and related constructive and destructive interference on the vertical and the horizontal components of motion. We plan to expand the available noise dataset and improve our understanding and interpretation of the difference between ambient noise and earthquake signals by utilizing recordings on the Japanese seismic network.

Some differences in V/H existed when analyzing the Swiss and Japanese datasets. One explanation for this difference could be the composition of the wave fields, which is related to the peculiarities of the sites in the particular region (e.g., the influence of sedimentary basins and topography). Swiss sites have a tendency to be close to theoretical rock sites where body waves, in particular P waves, might contribute more to the wave field at high frequency, whereas Japanese sites include a number of sites close to or in deep basins in which surface-wave excitation might significantly contribute to the wave field. A further reason for the small differences in V/H could be a measurement bias of the velocity profiles in the two datasets. Within the Network of Research Infrastructures for European Seismology project, active and passive seismic experiments were performed and compared at 19 sites selected in Italy, Greece, and Turkey (Bard *et al.*, 2010; Fäh *et al.*, 2010). The comparison proved good for all sites with V_{S30} lower than 500 m/s; at stiffer sites, velocity values estimated with surface-wave techniques (both passive and active) were smaller than those derived from borehole measurements. This observation is consistent with the previous comparison results reported by Moss (2008), and can explain the difference in the V/H relations for Switzerland and Japan. One of the main reasons for the different results is that borehole logging, as applied for the Japanese sites, and seismic measurements with surface waves, as applied for the Swiss sites, are performed in two different frequency ranges. This influences the level of heterogeneities that are resolved by the waves and thus might lead to differences in results. Further work is needed to provide a conclusive answer.

Data and Resources

Velocity profiles from ambient noise and multichannel analysis of surface waves are part of the site characterization database of the Swiss Seismological Service (SED; available upon request). The Swiss earthquake recordings used for defining site V/H ratios have been extracted from the recording database of SED through AutoDRM (http://www.seismo.ethz.ch/prod/autodrm/index_EN, last accessed July 2011). The Japanese earthquake data and velocity profiles are available through the Japanese National Research Institute for Earth Science and Disaster Prevention (NIED) ftp service (http://www.kik.bosai.go.jp, last accessed July 2011).

Acknowledgments

We thank the Japanese National Research Institute for Earth Science and Disaster Prevention for making waveform and velocity profile data available. This work was funded partly by swissnuclear and the Swiss Federal Nuclear Safety Inspectorate (ENSI). We extend our thanks to Associate Editor Samik Sil and two anonymous reviewers.

References

Abrahamson, N. A., and W. J. Silva (2008). Summary of the Abrahamson & Silva NGA ground-motion relations, *Earthq. Spectra* **24,** 67–97.

Akkar, S., and J. J. Bommer (2006). Influence of long-period filter cut-off on elastic spectral displacements, *Earthq. Eng. Struc. Dynam.* **35,** 1145–1165, ISSN 0098-8847.

Akkar, S., and J. J. Bommer (2010). Empirical equations for the prediction of PGA, PGV and spectral accelerations in Europe, the Mediterranean region and the Middle East, *Seismol. Res. Lett.* **81,** 195–206.

Alatik, L., N. Abrahamson, J. J. Bommer, F. Scherbaum, F. Cotton, and N. Kuehn (2010). The variability of ground-motion prediction models and its components, *Seismol. Res. Lett.* **81,** 794–801, doi10.1785/gssrl.81.5.794.

Albarello, D., and E. Lunedei (2009). Alternative interpretations of horizontal to vertical spectral ratios of ambient vibrations: New insights from theoretical modelling, *Bull. Earthq. Eng.* **8,** 519–534, doi 10.1007/s10518-009-9110-0.

Aoi, S., T. Kunugi, and H. Fujiwara (2004). Strong-motion seismograph network operated by NIED: K-Net and KiK-Net, *J. Japan Assoc. Earthq. Eng.* **4,** 65–74.

Bard, P.-Y., and M. Bouchon (1985). The two-dimensional resonance of sediment-filled valleys, *Bull. Seismol. Soc. Am.* **75,** 519–541.

Bard, P.-Y., H. Cadet, B. Endrun, M. Hobiger, F. Renalier, N. Theodulidis, M. Ohrnberger, D. Fäh, F. Sabetta, and P. Teves-Costa, *et al.* (2010). From non-invasive site characterization to site amplification: Recent advances in the use of ambient vibration measurements, *Earthq. Eng. Eur.—Geotech. Geol. Earthq. Eng.* **17,** 105–123, doi 10.1007/978-90-481-9544-2_5.

Bommer, J. J., S. Akkar, and Ö. Kale (2011). A model for vertical-to-horizontal response spectral ratios for Europe and the Middle East, *Bull. Seismol. Soc. Am.* **101,** 1783–1806.

Bonnefoy-Claudet, S., F. Cotton, and P.-Y. Bard (2006). The nature of noise wavefield and its applications for site effects studies: A literature review, *Earth Sci. Rev.* **79,** 205–227.

Boore, D. (2003). Simulation of ground motion using the stochastic method, *Pure Appl. Geophys.* **160,** 635–676.

Boore, D. M., and G. M. Atkinson (2008). Ground-motion prediction equations for the average horizontal component of PGA, PGV, and 5%-damped PSA at spectral periods between 0.01 s and 10.0 s, *Earthq. Spectra* **24,** 99–138.

Bozorgnia, Y., and K. W. Campbell (2004). The vertical-to-horizontal spectral ratio and tentative procedures for developing simplified V/H and vertical design spectra, *J. Earthq. Eng.* **4,** 539–561.

Building Seismic Safety Council (2003). The 2003 NEHRP recommended provisions for new buildings and other structures, Part 1: Provisions (FEMA 450), www.bssconline.org (last accessed October 2011).

Burjánek, J., G. Gassner-Stamm, V. Poggi, J. R. Moore, and D. Fäh (2010). Ambient vibration analysis of an unstable mountain slope, *Geophys. J. Int.* **180,** 820–828, doi 10.1111/j.1365-246X.2009.04451.x.

Capon, J. (1969). High-resolution frequency-wavenumber spectrum analysis, *Proc. IEEE* **57,** 1408–1418.

Cauzzi, C., and E. Faccioli (2008). Broadband (0.05 to 20 s) prediction of displacement response based on worldwide digital records, *J. Seismol.* **12,** 453–475.

Chiou, B. S.-J., and R. R. Youngs (2008). An NGA model for the average horizontal component of peak ground motion and response spectra, *Earthq. Spectra* **24,** 173–215, doi 10.1193/1.2894832.

Chiou, B., R. Darragh, N. Gregor, and W. Silva (2008). NGA project strong-motion database, *Earthq. Spectra* **24,** 23–44.

Deichmann, N., J. Clinton, S. Husen, B. Edwards, F. Haslinger, D. Fäh, *et al.* (2010). Earthquakes in Switzerland and surrounding regions during 2009, *Swiss J. Geosci.* **103,** 535–549, doi 10.1007/s00015-010-0039-8.

Douglas, J., and D. M. Boore (2010). High-frequency filtering of strong-motion records, *Bull. Earthq. Eng.* **9,** 395–409, doi 10.1007/s10518-010-9208-4.

Drouet, S., F. Cotton, and P. Guéguen (2010). V_{S30}, κ, regional attenuation and M_w from accelerograms: Application to magnitude 3 to 5 French earthquakes, *Geophys. J. Int.* **182,** 880–898.

Edwards, B., and A. Rietbrock (2009). A comparative study on attenuation and source-scaling relations in the Kantō, Tokai, and Chubu regions of Japan, using data from Hi-Net and KiK-Net, *Bull. Seismol. Soc. Am.* **99,** doi 10.1785/0120080292.

Edwards, B., B. Allmann, D. Fäh, and J. Clinton (2010). Automatic computation of moment magnitudes for small earthquakes and the scaling of local to moment magnitude, *Geophys. J. Int.* **183,** 407–420, doi 10.1111/j.1365-246X.2010.04743.x.

Edwards, B., A. Rietbrock, J. J. Bommer, and B. Baptie (2008). The acquisition of source, path and site effects from micro-earthquake recordings using Q tomography: Application to the UK, *Bull. Seismol. Soc. Am.* **98,** 1915–1935.

Fäh, D., and P. Huggenberger (2006). INTERREG III, Erdbebenmikrozonierung am südlichen Oberrhein. Zusammenfassung für das Projektgebiet Gebiet in der Schweiz, CD and report, 32 pp. (in German; available from the authors).

Fäh, D., S. Fritsche, V. Poggi, G. Gassner-Stamm, P. Kästli, J. Burjanek, P. Zweifel, S. Barman, J. Clinton, L. Keller, P. Renault, and S. Heuberger (2009). Determination of Site Information for Seismic Stations in Switzerland, *Swiss Seismological Service Technical Report: SED/PRP/R/004/20090831*, for the swissnuclear Pegasos Refinement Project, 121 pp.

Fäh, D., F. Kind, and D. Giardini (2001). A theoretical investigation of average H/V ratios, *Geophys. J. Int.* **145,** 535–549, doi 10.1046/j.0956-540x.2001.01406.x.

Fäh, D., V. Poggi, S. Marano, C. Michel, J. Burjánek, P.-Y. Bard, C. Cornou, M. Wathelet, F. Renalier, M. Hobiger, H. Cadet, M. Ohrnberger, B. Endrun, A. Savvaidis, N. Theodulidis, M. Kristekova, S. Hailemikael, and F. Sabetta, *et al.* (2010). Guidelines for the implementation of ambient vibration array techniques: Measurement, processing and interpretation, NERIES deliverable JRA4-D9, http://www.neries-eu.org (last accessed October 2011).

Fäh, D., G. Stamm, and H. B. Havenith (2008). Analysis of three-component ambient vibration array measurements, *Geophys. J. Int.* **172,** 199–213.

Fäh, D., M. Wathelet, M. Kristekova, H. Havenith, B. Endrun, G. Stamm, V. Poggi, J. Burjánek, and C. Cornou (2009). Using Ellipticity Information for Site Characterisation, *NERIES JRA4 "Geotechnical Site Characterization", Task B2-D4, Final Report.*

Fujiwara, H., S. Aoi, T. Kunugi, and S. Adachi (2004). Strong-motion observation networks of NIED: K-NET and KiK-net, http://www.cosmos-eq.org/events/wkshop_records_processing/papers/Fujiwara_paper.pdf, COSMOS (last accessed July 2011).

Gülerce, Z., and N. Abrahamson (2010). Vector-valued probabilistic seismic hazard assessment for the effects of vertical ground motions on the seismic response of highway bridges, *Earthq. Spectra* **26,** 999–1016, doi 10.1193/1.3464548.

Gülerce, Z., and N. Abrahamson (2011). Site-specific design spectra for vertical ground-motion, *Earthquake Spectra* **27,** no. 4 (in press).

Hagshenas, E., P.-Y. Bard, and N. TheodulidisSESAME WP04 Team (2008). Empirical evaluation of microtremor H/V spectral ratio, *Bull. Earthq. Eng.* **6,** 75–108.

Havenith, H. B., D. Fäh, U. Pollom, and A. Roulle (2007). *S*-wave velocity measurements applied to the seismic microzonation of Basel, Upper Rhine graben, *Geophys. J. Int.* **170,** 346–358.

Hobiger, M., P.-Y. Bard, C. Cornou, and N. Le Bihan (2009). Single station determination of Rayleigh wave ellipticity by using the random decrement technique (RayDec), *Geophys. Res. Lett.* **36,** L14303, doi 10.1029/2009GL038863.

Joyner, W. B., R. E. Warrick, and T. E. Fumal (1981). The effect of Quaternary alluvium on strong ground motion in the Coyote Lake, California, earthquake of 1979, *Bull. Seismol. Soc. Am.* **71,** 1333–1349.

Köhler, A., M. Ohrnberger, F. Scherbaum, M. Wathelet, and C. Cornou (2007). Assessing the reliability of the modified three-component spatial autocorrelation technique, *Geophys. J. Int.* **168,** 779–796.

Kunnath, S. K., E. Erduran, Y. H. Chai, and M. Yashinsky (2008). Effect of near-fault vertical ground motions on seismic response of high overcrossings, *J. Bridge Eng.* **13,** 282–290.

Malhotra, P. K. (2006). Smooth spectra of horizontal and vertical ground motions, *Bull. Seismol. Soc. Am.* **96,** 506–518.

McGuire, R. K., W. J. Silva, and C. J. Costantino (2001). Technical Basis for Revision of Regulatory Guidance on Design Ground Motions: Hazard- and Risk-Consistent Ground Motion Spectra Guidelines, *NUREG/CR-6728*, U. S. Nuclear Regulatory Commission, Washington, D.C., 213 pp.

Moss, R. E. S. (2008). Quantifying measurement uncertainty of thirty-meter shear-wave velocity, *Bull. Seismol. Soc. Am.* **98,** 1399–1411, doi 10.1785/0120070101.

Nakamura, Y. (1989). A method for dynamic characteristics estimation of subsurface using microtremor on the ground surface, *Q. Rep. Railway Tech. Res. Inst.* **30,** 25–33.

Newmark, N. M., and W. J. Hall (1969). Seismic design criteria for nuclear reactor facilities, *Proc. of the 4th World Conf. on Earthquake Engineering*, Santiago, Chile, 13–18 January 1969, B4, 37–50; International Association for Earthquake Engineering in Tokyo (IAEE), available at http://www.nicee.org/wcee/.

Newmark, N. M., and W. J. Hall (1982). Earthquake spectra and design, *EERI Monograph 3*, Earthquake Engineering Research Institute, Oakland, California, 103 pp.

Nogoshi, M., and T. Igarashi (1971). On the amplitude characteristics of microtremors. Part 2, *J. Seismol. Soc. Japan* **24,** 26–40 (in Japanese with English abstract).

Park, C. B., R. D. Miller, and J. Xia (1999). Multichannel analysis of surface waves, *Geophysics* **64,** 800–808.

Poggi, V., and D. Fäh (2010). Estimating Rayleigh wave particle motion from three-component array analysis of ambient vibrations, *Geophys. J. Int.* **180,** 251–267, doi 10.1111/j.1365-246X.2009.04402.x.

Poggi, V., B. Edwards, and D. Fäh (2011). Derivation of a reference shear-wave velocity model from empirical site amplification, *Bull. Seismol. Soc. Am.* **101,** 258–274.

Raoof, M., R. B. Herrmann, and L. Malagnini (1999). Attenuation and excitation of three component ground motion in southern California, *Bull. Seismol. Soc. Am.* **89,** 888–902.

Renault, P., S. Heuberger, and N. A. Abrahamson (2010). PEGASOS Refinement Project: An improved PSHA for Swiss nuclear power plants, Paper Number 991, in *Proc. of the 14ECEE—European Conf.*

of Earthquake Engineering, Ohrid, Republic of Macedonia, 30 August–3 September 2010.

Roten, D., D. Fäh, C. Cornou, and D. Giardini (2006). Two-dimensional resonances in Alpine valleys identified from ambient vibration wavefields, *Geophys. J. Int.* **165,** 889–905.

Scherbaum, F., K. G. Hinzen, and M. Ohrnberger (2003). Determination of shallow shear wave velocity profiles in the Cologne Germany area using ambient vibrations, *Geophys. J. Int.* **152,** 597–612.

Yamanaka, H., M. Takemura, H. Ishida, and M. Niea (1994). Characteristics of long-period microtremors and their applicability in exploration of deep layers, *Bull. Seismol. Soc. Am.* **84,** 1831–1841.

Zhao, J. X., J. Zhang, A. Asano, Y. Ohno, T. Oouchi, T. Takahashi, H. Ogawa, K. Irikura, H. K. Thio, P. G. Somerville, Y. Fukushima, and Y. Fukushima (2006). Attenuation relations of strong ground motion in Japan using site classification based on predominant period, *Bull. Seismol. Soc. Am.* **96,** 898–913.

Swiss Seismological Service
Sonneggstrasse 5
ETH Zürich
Zürich, Switzerland
edwards@sed.ethz.ch

Manuscript received 19 January 2011